Supplementary Materials for

In vivo gene editing in dystrophic mouse muscle and muscle stem cells

Mohammadsharif Tabebordbar, Kexian Zhu, Jason K.W. Cheng, Wei Leong Chew, Jeffrey J. Widrick, Winston X. Yan, Claire Maesner, Elizabeth Y. Wu, Ru Xiao, F. Ann Ran, Le Cong, Feng Zhang, Luk H. Vandenberghe, George M. Church, Amy J. Wagers*

*Correspondence to: amy_wagers@harvard.edu

This PDF file includes:

Supplementary Materials

Materials and Methods

Constructs

Plasmid encoding SpCas9 and the Sp gRNA cloning plasmid were generated by the Church lab. Sp gRNA plasmids targeting Ai9 and *Dmd*23 loci were derived from the parental construct by amplifying the plasmid using a forward primer that includes the gRNA target sequence in the 5' end and anneals to the gRNA scaffold in the 3' end along with a reverse primer that anneals to the 3′ end of the U6 promoter. Target sequences of the gRNAs are provided in Table S1. PCR products were treated with DpnI (NEB), purified using QIAquick PCR Purification Kit (Qiagen), phosphorylated with T4 Polynucleotide Kinase (NEB), self-ligated using the Quick Ligation Kit (NEB) and transformed into Top10 competent cells (LifeTech). Individual colonies were analyzed by Sanger sequencing. Coupled Ai9-*Dmd*23 Sp gRNAs were generated from the single Sp gRNA plasmids using standard restriction enzyme and ligation-based cloning methods. Plasmid encoding SaCas9 and the Sa gRNA cloning plasmids were gifts from Feng Zhang. Sa gRNA plasmids targeting Ai9 and *Dmd*23 loci were derived from the parental constructs using the same strategy as the Sp gRNA plasmids.

The 173CMV_SaCas9_Ai9/*Dmd*23 gRNAs constructs were generated by isothermal assembly of 4 fragments using Gibson Assembly Master Mix (NEB). 173CMV promoter followed by SaCas9 was amplified from Zhang lab plasmid using primers 173cmv_f and saCas9_r (Table S3). Two gBlocks each were synthesized (IDT) to together cover SV40-polyA, U6 promoter, left gRNA, U6 promoter, right gRNA for Ai9 and *Dmd23* guides, respectively (Table S4). gBlocks were PCR amplified using gBlock_f and gBlock_r primers and digested with BbsI (NEB). The final piece, pUC19 backbone, was PCR amplified with pUC19_f and pUC19_r from pUC19 control

plasmid (LifeTech). All PCR products were gel extracted prior to Gibson Assembly. EFS_SaCas9_Ai9/*Dmd*23 gRNAs constructs were similarly constructed with EFS promoter amplified from a plasmid containing full length EF1α promoter (a gift from John Rinn) with EFS_f and EFS_r primers, followed by SaCas9 amplified with primers SaCas9_f and SaCas9_r (Table S3) and the two gBlocks as well as the pUC19 backbone as previously mentioned. Correctly assembled plasmids were confirmed by Sanger sequencing and subsequently used to construct AAV plasmid with pZac2.1 backbone.

The pZac2.1 AAV backbone plasmid was purchased from University of Pennsylvania Vector Core. AAV constructs were inserted into the pZac2.1 backbone using a restriction enzyme digestion and blunt end ligation approach and transformed into Stbl3 competent cells (LifeTech).

Genomic DNA extraction and genomic PCR

Genomic DNA was extracted from tissues and *in vitro* cultured cells using Quick Extract solution (Epicentre) according to manufacturer's instruction. DNA samples in Quick Extract of volumes equal to 10% of the final PCR reaction were used. Phusion Human Specimen Direct PCR Kit (ThermoFisher) was used to amplify *Dmd*23 locus from the *in vitro* transfected satellite cell-derived myotubes using Genomic_Dmd23_f and Genomic_Dmd23_r primers (Table S2) with the following PCR condition: 98°C for 3 min, 6x [98°C for 5s, 68°C (-1°C/cycle) for 10s, 68°C for 1 min], 29x (98°C for 5s, 62°C for 10s, 68°C for 1 min), 68°C for 3 min.

Nested PCR was performed for locally injected TA muscles using Phusion Green Hot Start II High-Fidelity PCR Master Mix (ThermoFisher) with 20 cycles of first round amplification using above-mentioned primers and thermocycling conditions followed by 25 cycles of second round amplification using Genomic_Dmd23_nested_f and Genomic_Dmd23_nested_r (Table S2) with

a 1:10 dilution between the two rounds and the following conditions: 98°C for 3 min, 25x (98°C for 5s, 66°C for 10s, 72°C for 15s), 72°C for 5 min. Unedited and exon-excised bands were gel extracted and cloned into TOPO plasmids using Zero Blunt TOPO PCR cloning kit (LifeTech) and subsequently transformed into TOP10 competent cells. Individual colonies were analyzed by Sanger sequencing to confirm the correct excision of sequence flanked by two guide RNAs.

Next-Generation Sequencing for On- and Off-target Indel Frequencies of *Dmd*-targeting Sa gRNAs (DL2 and DR7)

The highest ranking candidate off-target sites were identified with a Zhang lab algorithm (*28*) using Benchling software for the Sa *Dmd* gRNAs DL2 and DR7. PCR was used to amplify the genomic regions flanking the predicted cutting sites in the mouse *Dmd* gene (on-target) and the top 8 predicted off-targets for DL2 and DR7, respectively (see Fig. S12). A second round of PCR was used to attach the Illumina P5 adapters as well as unique sample-specific barcodes to the target amplicons. PCR products were pooled and gel extracted twice using QIAquick Gel Extraction Kit (Qiagen). Barcoded and purified DNA samples were quantified by Nanodrop and pooled with an equimolar ratio. Sequencing libraries were sequenced with the Illumina MiSeq Personal Sequencer and insertion or deletion (indel) analyses was carried out as previously described (*28*).

RT-PCR and Taqman-based real time PCR

Total RNA was isolated from tissues using TRIzol reagent (LifeTech) per manufacturer's instructions. For tissues harvested from animals, 1ug of RNA was used for cDNA synthesis with SuperScript III First Strand Synthesis SuperMix (LifeTech) in 20uL reactions. For *in vitro*

cultured samples, 400ng of RNA was used for cDNA synthesis with SuperScript VILO MasterMix (LifeTech) in 20uL reactions. RT-PCR was performed using 1uL cDNA with Q5 HotStart MasterMix (NEB) using RT_Dmd23_f and RT_Dmd23_r (Table S2) primers with the following condition: 98°C for 3 min, 40x (98°C for 10s, 60°C for 15s, 65°C for 30s), 65°C for 3 min. Both unedited and exon23-deleted bands were gel extracted and cloned into TOPO vectors using Zero Blunt TOPO PCR cloning kit (LifeTech) and subsequently transformed into TOP10 competent cells. Individual colonies were analyzed by Sanger sequencing. Alignment to genomic sequence was performed using Geneious software. Taqman quantitative Real-Time PCR was performed as previously described (*9*). A taqman probe against exon4-5 junction was used for quantification of total *Dmd* transcripts, and another probe against exon22-24 junction was used for quantification of exon23-deleted transcripts (Table S2). A taqman assay for 18s ribosomal RNA was used as housekeeping control (ThermoFisher, Cat # 4333760). Assays were carried out in triplicates of 10uL reactions for each probe and with 20ng of cDNA input. Taqman Fast Advanced Master Mix (LifeTech) was used with fast cycling conditions recommended by the manual, 50°C for 2 min, 95°C for 20s, 40x (95°C for 1s, 60°C for 20s), with data collection at the end of each PCR cycle. Delta-Ct values between exon4-5 and exon22-24 were used to quantify the percentage of exon23-deleted transcripts in comparison to total *Dmd* transcripts.

Satellite cell isolation, culture and transfection

Satellite cell isolation from *mdx;Ai9* mice (for the *in vitro* transfection experiments) and mice systemically injected with AAV CRISPR was performed as previously described (*29, 30*). For satellite isolation from locally injected muscles, TA muscles were harvested and cut into small pieces using a curved scissor. Mononuclear cells were obtained by enzymatic digestion with

0.2% collagenase type II and 0.05% dispase in DMEM (LifeTech) at 37°C for 15 min followed by another 10 min digestion. The cells were centrifuged, filtered through a 70 um strainer and stained with the antibody mix (APCCy7-CD45 (BD, clone 30-F11, 1:200), APCCy7-CD11b (BD, clone M1/70, 1:200), APCCy7-TER119 (Biolegend, clone TER-119, 1:200). APC conjugated Sca-1 (eBioscience, clone D7, 1:200)) for 30 min on ice in HBSS (LifeTech) containing 2% Donor Bovine Serum (DBS). For isolating satellite cells from *Pax7-ZsGreen* $^{+/-}$ *;mdx;Ai9* mice, Zsgreen + cells were isolated after gating for live mononuclear cells lacking expression of Sca1, CD45, Ter119 and Mac1. For *in vitro* expansion of satellite cells isolated from AAV CRISPR injected muscles, satellite cells were seeded on collagen/laminin-coated plates in F10 (GIBCO) containing 20% donor horse serum (Atlanta Biologics), 1% penicillin-streptomycin (LifeTech), and 1% glutamax (Lifetech). 5 ng/ml bFGF (Sigma) was added to the medium daily. Medium was changed with fresh medium every other day. After 7 days, satellite cells were harvested, cell numbers were counted and cells were re-plated in multiple wells of a 96 well plate for differentiation. The next day, medium was changed to DMEM (GIBCO) containing 2% donor horse serum (Atlanta Biologics), 1% penicillin-streptomycin (LifeTech). Myotubes were fixed with 4% PFA or harvested in TriZol reagent for RNA analysis, in quick DNA extract for DNA analysis and in RIPA buffer for protein analysis after 60 or 72 hours in differentiation medium. Satellite cells from *mdx;Ai9* mice, used for *in vitro* transfection, were cultured on 6-well plates in the presence of forskolin (50 uM) for 5 days (*18*). On day 6, cells were harvested and re-plated in 10 cm dishes and transfected with plasmids encoding SpCas9 and gRNA plasmids using lipofectamine 3000 reagent per manufacturer's instructions. TdTomato+ gene-targeted cells were double-sorted 2 days after transfection and expanded in culture for 5 days before *in vitro* myogenic differentiation/*in vivo* transplantation.

Satellite cell transplantation

25 μl of Naja mossambica mossambica cardiotoxin (0.03 mg/ml, Sigma) was injected in the tibialis anterior (TA) muscle of anesthetized *mdx* mice 1 day before satellite cell transplantation. For transplant of *in vitro* transfected satellite cells, 300,000 *in vitro* transfected tdTomato+ satellite cells were injected directly into these pre-injured muscles, one day after cardiotoxin injection, in 50 μl PBS. For transplantation with satellite cells isolated from dystrophic muscles injected intramuscularly with AAV-Ai9 CRISPR, 200,000 satellite cells (including tdTomato+ gene-edited cells), which were expanded in culture for two weeks, were injected. Muscles transplanted with *in vitro* transfected satellite cells were harvested 3 weeks after injection, and muscles transplanted with satellite cells from intramuscular AAV-Ai9 CRISPR injected muscles were harvested 10 days after transplantation for cryosectioning and immunofluorescence/epifluorescence analysis.

AAV Production

CRISPR AAVs were generated through the Gene Transfer Vector Core (GTVC) at the Grousbeck Gene Therapy Center at the Schepens Eye Research Institute and Massachusetts Eye and Ear Infirmary(SERI/MEEI). AAV9 encoding Cre was purchased from University of Pennsylvania Vector Core.

Western blotting:

Protein was extracted from tissues and cultured cells using RIPA buffer (Cell Signaling). Tissues were homogenized using GentleMACS M-tubes (Miltenyi Biotech) with protein 1.1 program. Protein was concentrated using Amicon Ultra 10k centrifugal filter units. Protein concentration

was determined by BCA assay (Pierce). 25ug, 25ug, 50 ug and 50ug of total protein per lane were used for myotubes, locally injected TA muscles, muscles from IP injected mice and muscles from systemically injected adult mice, respectively. Different percentages of wild-type muscle proteins were diluted in *mdx* proteins from the same muscle type so that the total protein of that lane was kept the same. Samples were denatured at 99°C for 5 minutes before being loaded on to 4-20% Tris-HCl precast Criterion gels (Bio-Rad). DYSTROPHIN and GAPDH (loading control) were detected by primary antibodies NCL_DYS1 (1:100, Novocastra) and sc-32233 (1:25,000, Santa-Cruz Biotechnology) followed by horse anti-mouse IgG HRP-linked (1:1,000, Cell Signaling Technology 7076P2). ChemiDoc imaging system (Bio-Rad) was used to detect chemiluminescence after using Supersignal west Dura ECL kit (ThermoFisher). Intensity of DYSTROPHIN and GAPDH bands were quantified using ImageJ gel analysis function. Within a particular experiment, it was sometimes necessary to quantify using different exposure times for DYSTROPHIN versus GAPDH, in order to ensure that quantification was performed in the linear range for each protein. In all cases, all samples being compared were exposed equivalently for a given protein target. The relative abundance of DYSTROPHIN in total protein was evaluated semi-quantitatively by the ratio of DYSTROPHIN and GAPDH signals and is presented in Arbitrary Units (A.U.). Detection of multiple bands for DYSTROPHIN with NCL-Dys1 antibody is consistent with previous reports in literature (*10, 31, 32*).

Detection of DYSTROPHIN by capillary immunoassay (Simple Western)

Protein was extracted and processed as described for Western blotting (above). The Wes 66-440 kDa Mouse Master Kit (PS-MK09) was used for all Simple Western experiments on the ProteinSimple Wes system. Specifically, 5uL of protein extract from each sample was loaded to

the kit at the final concentration of 2ug/uL. DYSTROPHIN and Vinculin (loading control) were detected by primary antibodies NCL_DYS1 (1:100, Novocastra) and MAB6896 (1:12.5, R&D). Goat Anti-Mouse Secondary HRP Conjugate (ready-to-use reagent) was used according to manufacturer's instructions (ProteinSimple). Default running and detection programs were used across all the assays (Separation time 30 minutes, Separation Voltage 475 Volts, Antibody Diluent time 5 minutes, Primary Antibody time 30 minutes, Secondary Antibody time 30 minutes). Compass software (ProteinSimple) was used to visualize virtual gels. Relative protein quantification was generated from chromatograms of the indicated samples.

Histology and immunofluorescence:

Mouse skeletal and heart muscles were dissected. Samples used for DYSTROPHIN immunofluorescence were embedded in O.C.T compound (Tissue-Tek) immediately after dissection and frozen in liquid-nitrogen-cold isopentane. Sample used for tdTomato epifluorescence were fixed in 4% PFA for 1 h at room temperature and immersed in 30% sucrose until submersion, before embedding in O.C.T. and freezing. For DYSTROPHIN immunostaining of *mdx* muscle sections transplanted with tdTomato+ satellite cells, tissues were fixed in 2% PFA for 30 min before embedding in O.C.T. and freezing. Subsequent cryosectioning was performed using a Microm HM550 (Thermo Scientific) at the thickness of 12 μm for skeletal muscles and 30 um for heart. For DYSTROPHIN, nNos and Syntrophin immunostaining, cryosections were blocked with 5% Normal Goat Serum (NGS) (Jackson ImmunoResearch), 2% Bovine Serum Albumin (BSA) (Sigma), 2% protein concentrate (M.O.M. Kit, Vector Laboratories, BMK-2202), and 0.1% tween-20 (Sigma) for 1h at room temperature, followed by 2 x 5 min DPBS washes. Sections were subsequently stained with rabbit polyclonal anti-dystrophin (1:50,

Abcam, ab15277), rabbit polyclonal anti-nNos (1:100, Immunostar, 24431) or rabbit monoclonal anti-Syntrophin (1:200, Abcam, ab11187) antibody at 4°C overnight, followed by 4 x 5min DPBS washes each. Slides were then incubated with secondary goat-anti-rabbit IgG Alexa Fluor 488 (1:250, LifeTech) at room temperature for 1 h, followed by 4 x 5 min DPBS washes. Slides were then mounted with mounting media containing DAPI (Vector Laboratories).

For alpha-Sarcoglycan, beta-Sarcoglycan, beta-Dystroglycan and Dystrobrevin stainings, cryosections were blocked with 5% Normal Goat Serum (NGS) (Jackson ImmunoResearch), 2% Bovine Serum Albumin (BSA) (Sigma), 2% protein concentrate (M.O.M. Kit, Vector Laboratories, BMK-2202), 1 drop/ml of M.O.M. blocking reagent (M.O.M. Kit, Vector Laboratories, BMK-2202) and 0.1% tween-20 (Sigma) for 1h at room temperature, followed by 2 x 5 min DPBS washes. Sections were subsequently stained with mouse monoclonal anti-alpha Sarcoglycan (1:50, abcam, ab49451), anti-beta Sarcoglycan (1:100, Novacastra, NCL-L-b-SARC), anti-beta Dystroglycan (1:100, Novacastra, NCL-b-DG) or anti-Dystrobrevin (1:100, BD Biosciences, 610766) antibody, at 4°C overnight, followed by 4 x 10 min DPBS washes each. Slides were then incubated with secondary goat-anti-mouse IgG Alexa Fluor 488 (1:250, LifeTech) at room temperature for 1 h, followed by 4 x 10 min DPBS washes. Slides were then mounted with mounting media containing DAPI (Vector Laboratories).

For LAMININ staining, sections were fixed on the slide using 4% PFA for 10 min, washed with DPBS for 3 x 5 min, blocked and stained with a rabbit polyclonal anti-laminin antibody (1:200, Millipore, AB2034) as described above for the DYSTROPHIN staining. For MHC staining of *in vitro* differentiated myotubes, myotubes were permeablized using 0.5% TritonX-100 (Sigma) for 15 min at RT, washed 2 x 5 min with DPBS, blocked with 5% NGS, 2% BSA, 2% protein concentrate, and 0.1% tween-20 for 1h at room temperature, washed 2 x 5 min with DPBS,

incubated with anti-skeletal myosin type II (fast-twitch) (1:200, Sigma) and anti-skeletal myosin type I (slow-twitch) (1:100, Sigma) at 4°C overnight, washed 4 x 5min with DPBS, incubated with goat anti-mouse IgG Alexa-488 conjugate secondary antibody (1:250, LifeTech), washed 4 x5 min with DPBS and stained with 10 mg/ml Hoechst (Invitrogen). 12 μm sections were fixed in 4% PFA for 10 min and washed with DPBS for 3 x 5 min before H&E staining.

Mice

Animal care and experimental protocols were approved by the Harvard University Institutional Animal Care and Use Committee (IACUC). *Mdx* mice (JAX, #001801) were bred with Ai9 mice (JAX, #007905) in the Harvard Biological Research Infrastructure to generate the *mdx;Ai9* mice. *Pax7-ZsGreen* mice (kindly provided by Dr. Michael Kyba, University of Minnesota) were bred with *mdx; Ai9* mice to generate the *Pax7-ZsGreen* $^{+/-}$*;mdx;Ai9* mice. Wild type C57BL6/J mice (JAX, #000664) were purchased from Jackson laboratories.

AAV injections

For intramuscular injections into adult mice, animals were anesthetized using isoflurane and virus was injected into the TA muscle (6E+11 vg for AAV-Cre or 1.5E+12 vg for AAV CRISPR). For systemic injections into neonatal mice, virus was injected intraperitoneally (3E+11 vg for AAV-Cre or 3E+12 vg for AAV CRISPR) to mice on postnatal day 3 (P3). For adult systemic injections, virus was injected via tail vein (3.6E+13 vg/mouse).

Analyzing muscle contractile properties:

Mice were anesthetized with sodium pentobarbital (80-100 mg/kg body mass). Supplemental doses were provided as necessary during the experiment. Small incisions were made to expose the right tibialis anterior (TA) tendon and right patellar tendon. The mouse was placed on the temperature-controlled platform (38 °C) of an in situ test stand (Aurora Scientific model 809B, Aurora, Ontario, Canada). Silk suture (4-0) was used to attach the severed TA tendon to the lever arm of a dual mode muscle lever system (Aurora Scientific model 305C-LR). The lower right limb was stabilized by using suture attached to the patellar tendon to secure the knee to a horizontal support. Supramaximal 200 μs square-wave pulses, output by a high current muscle stimulator (Aurora Scientific, model 701A), were delivered to platinum electrodes inserted behind the knee to depolarize the peroneal nerve. The lever system was interfaced to a PC using a multi-function data acquisition board (National Instruments model USB-6229, Austin, TX). Custom software written in LabVIEW (National Instruments) was used to configure and trigger stimulation, control lever arm position, and record data to disk. After the right leg was studied, the animal was removed from the test stand and the left leg prepared and studied in an identical manner. All contractile measurements were initiated at the empirically determined optimal length (L_0) for tetanic tension (200 Hz stimulation). Fiber length (FL) was calculated as 0.60 L_0 (*33*). Susceptibility to mechanical strain was evaluated by subjecting the muscle to 5 lengthening (eccentric) trials. During each lengthening trial the muscle was tetanically stimulated at L_0 for 100 ms and then lengthened to 1.20 FL at a velocity of +1.5 FL/s. Stimulation ceased at the conclusion of the lengthening ramp. The muscle was held for 200 ms before being returned to its L_0 at a velocity of -1.5 FL/s. The series of lengthening contractions was bracketed by fixed-end tetanic contractions, which were used to evaluate the overall change in force due to the lengthening contractions. One minute separated all contractions.

Specific force was calculated as active tetanic force divided by physiological cross-sectional area (pCSA). The pCSA of the TA was calculated as muscle mass divided by the product of FL and muscle density. Muscle density was taken as 1.06 mg/mm^3 (*34*).

Supplementary text

Rationale for the use of gene-editing approaches to restore DYSTROPHIN function in DMD. *DMD* encodes the muscle structural protein DYSTROPHIN, which functions normally to link the cytoskeleton of muscle fibers to the extracellular matrix, providing structural stability and protection from contraction-mediated damage (*35, 36*). Loss of DYSTROPHIN function causes frequent myofiber degeneration that ultimately outpaces fiber replacement by regenerative muscle stem cells (satellite cells) (*37*), which further exhibit profound, cell-intrinsic defects that reduce their capacity to contribute to muscle regeneration (*38*). Current therapies for DMD are very limited, and focus mainly on managing symptoms. Current strategies aimed at improving treatment options are predicated on the assumption that even partial restoration of DYSTROPHIN expression and/or function in affected cell types would ameliorate disease pathology. Some of the strongest evidence in support of this notion comes from studies using antisense oligonucleotides (AONs) to mask DMD splice donor and acceptor sequences in order to "skip" mutated exons and restore DYSTROPHIN reading frame. Indeed, studies in *mdx* mice, which carry a nonsense mutation in *Dmd* exon23, have demonstrated that AON-mediated skipping of exon23 produces an internally truncated, but still highly functional protein that can complement DYSTROPHIN-deficiency in dystrophic muscle (*5*). Similar strategies have been applied in human patients and show some promise, although they have failed to meet predetermined clinical endpoints, likely reflecting insufficient rescue of DYSTROPHIN protein expression in key target tissues (*39*). Indeed, while progress has been made recently through the use of tricyclo-DNA (tcDNA) and Pip5 transduction peptide-based approaches (*9, 40*), early AON chemistries induced relatively low levels of exon skipping in skeletal muscles and were particularly inefficient at delivery to cardiac muscle. Furthermore, even with relatively stable

chemistries (*9*), AONs have a defined half-life (*9, 10*), requiring patients to undergo repeated rounds of treatment. This need for multiple injections increases both the cost and potential side effects of AON therapy. Finally, delivery of AONs of any chemistry to resident muscle satellite cells, if it occurs, is likely to be ineffective because the AONs are diluted during proliferation. Strategies in which AONs are delivered virally, by embedding within small nuclear RNAs, suffer similarly from progressive loss of the viral genome, and its encoded AONs, from dystrophic muscles (*41*). Thus, ironically, in the context of gene therapy for DMD, the regenerative activities of muscle satellite cells pose a potential threat to therapeutic DYSTROPHIN restoration, as the addition of new, non-targeted nuclei would reduce the fraction of myonuclei in muscle fibers producing therapeutic exon skipped mRNA or shortened forms of DYSTROPHIN. Of course, on the other hand, successful targeting of satellite cells *in vivo* would provide a mechanism for continual replenishment of gene-edited myonuclei through normal muscle repair mechanisms, and may be important to correct satellite cell-intrinsic polarity defects arising from DYSTROPHIN loss-of-function (*38*).

It was with these considerations in mind that we sought to adapt the gene-editing potential of the CRISPR/Cas9 system, which enables irreversible modification of targeted gene loci, for enduring production of functional DYSTROPHIN protein in dystrophic heart, muscle and satellite cells. Our data, described in this manuscript, provide exciting support in DMD model mice for recovery of DYSTROPHIN expression and function in dystrophic skeletal muscle, cardiac muscle, and satellite cells, through local or systemic dissemination of gene editing complexes targeting the *Dmd* locus. As it has been estimated that more than 60% of DMD patients could benefit from skipping one or more exons in the exon 45-55 region (*42, 43*), clinical translation of our strategy, which employs a clinically relevant AAV delivery strategy,

already in use in human trials (*44, 45*), has the potential to transform the clinical course of disease for a significant number of DMD patients. Given that an accompanying manuscript by Gersbach and colleagues describes similar application of AAV8 to target *Dmd* by CRISPR-mediated gene editing in muscle fibers, it appears that this approach can be successful with other muscle-targeting AAV serotypes and other gRNA targets (*46*), and may be broadly applicable to address any of a number of genomic lesions underlying human muscle pathologies.

Still, the AAV-CRISPR system will require further optimization in order to realize its translational potential, in particular to identify additional AAV subclasses with optimal tropism for muscle satellite cells and reduced immunogenicity (*47*). Further studies also are needed to evaluate the long-term safety of the *in vivo* AAV-CRISPR approach, although the relative improvements seen in muscle function and minimal off-target effects (Fig. S12) seen in both our study and accompanying manuscript by Gersbach (*46*) argues against any severe, acute detrimental effects. Finally, with regard to the human disease, future identification of Sa gRNAs optimized for maximal on-target and minimal off-target activity at broadly relevant DMD mutations (including mutational 'hotspots' in the exon 45-55 region) could enable rapid translation of the results from our studies for the many DMD patients who could potentially benefit from this approach.

Supplementary Figures (S1-S12)

Supplementary Figure Legends

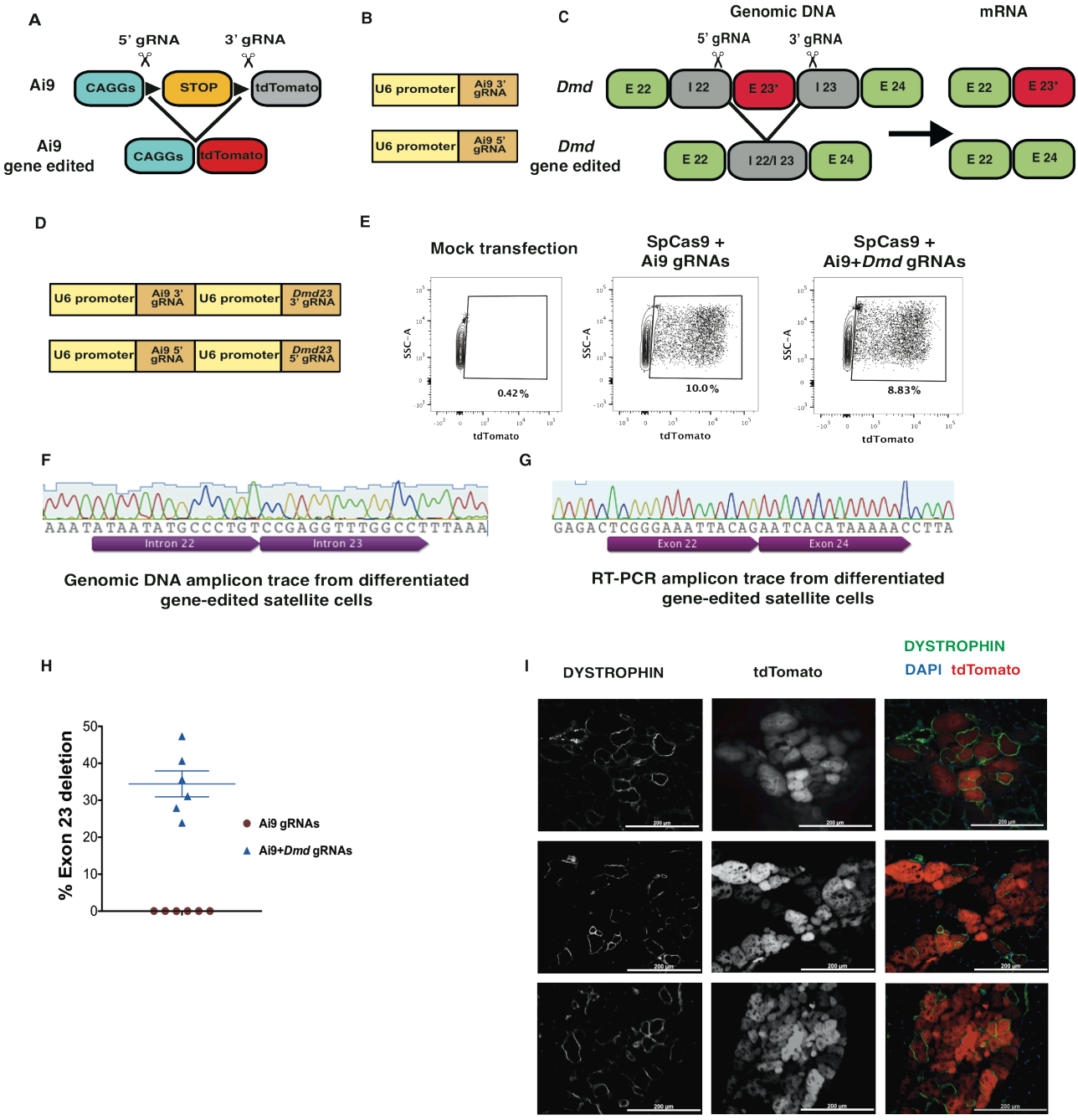

Figure S1. A sensitive, fluorescence-based reporter system for detection and enrichment of gene-edited *mdx;Ai9* satellite cells.

(**A**) Schematic of the Ai9 allele and its use as a fluorescent CRISPR activity reporter. Programming of Cas9 with paired gRNAs directed at the 5' and 3' loxP sites of the Ai9 allele results in excision of the intervening DNA, which encodes a termination sequence (STOP), and enables expression of the downstream tdTomato transgene. This system provides sensitive, fluorescence-based detection of CRISPR activity with single cell resolution and the capacity to prospectively detect and isolate gene-edited cells and their progeny by fluorescence activated cell sorting (FACS).

(**B**) Schematics of Ai9 targeting gRNA constructs.

(**C**) Schematic of CRISPR-mediated excision of *Dmd* exon23. In *mdx* mice, a nonsense mutation in exon23 (E23*) results in truncation and destabilization of the *Dmd* mRNA and loss of DYSTROPHIN protein expression (*17*). Programming of Cas9 with paired gRNAs directed at sequences 5' and 3' of exon23 directs excision of the intervening DNA, including the mutated exon23, and produces a fused Intron 22/23 (I 22/23). Transcription and splicing of this gene-edited *Dmd* locus generates an exon23-deleted mRNA that can be translated to produce an internally truncated, but still highly functional protein that has been shown to complement DYSTROPHIN-deficiency in dystrophic muscle (*5*).

(**D**) Schematics of coupled Ai9-*Dmd23* gRNA constructs in which the 3' gRNAs for Ai9 and *Dmd* are encoded in one vector and the 5' gRNAs in another. This system effectively links expression of the CRISPR activity reporter (tdTomato) to genome editing events at the *Dmd* locus because in order to express tdTomato after co-transfection with these vectors and SpCas9,

the target cell must have received both the 5' and 3' Ai9 gRNAs, and therefore must also have received both of the linked *Dmd*23 gRNAs.

(**E**) Representative FACS plots from *mdx;Ai9* satellite cells transfected with plasmids encoding SpCas9 and Ai9-*Dmd*23 coupled gRNAs (right panel), SpCas9 and Ai9 gRNAs (middle panel), or no plasmids (left panel). Gene-editing activity in cells receiving Ai9 or Ai9-*Dmd*23 coupled gRNAs is reported by tdTomato fluorescence.

(**F**) Sanger sequencing of amplicons confirms exon23 deletion and generation of a fused intron 22/23 in genomic DNA from myotubes derived from *mdx;Ai9* satellite cells transfected with SpCas9 and coupled Ai9-*Dmd*23 gRNAs. A representative trace is shown from the sample at the far right of the gel in Fig. 1A (red asterisk).

(**G**) Sanger sequencing of RT-PCR amplicons confirms production of an exon23-deleted mRNA transcript, in which exon22 is followed in frame by exon24, in myotubes derived from *mdx;Ai9* satellite cells transfected with SpCas9 and coupled Ai9-*Dmd*23 gRNAs. A representative trace is shown from the sample at the far right of the gel in Fig. 1B (blue asterisk).

(**H**) Quantification of percent exon23-deleted transcripts in satellite cell-derived myotubes by Taqman-based real-time PCR. Data are plotted as individual data points for Ai9 gRNAs (red) or Ai9-*Dmd*23 coupled gRNAs (blue) and overlaid with mean +/- SEM (n=6 transfections analyzed per group).

(**I**) Additional examples of DYSTROPHIN immunofluorescence in *mdx* muscles transplanted with satellite cells transfected *ex vivo* with SpCas9 + Ai9-*Dmd*23 coupled gRNAs. Black and white images are provided for DYSTROPHIN and tdTomato for better visualization. For the merged image: Green: DYSTROPHIN; Red: tdTomato; Blue: DAPI (nuclei). Scale bar: 200 um.

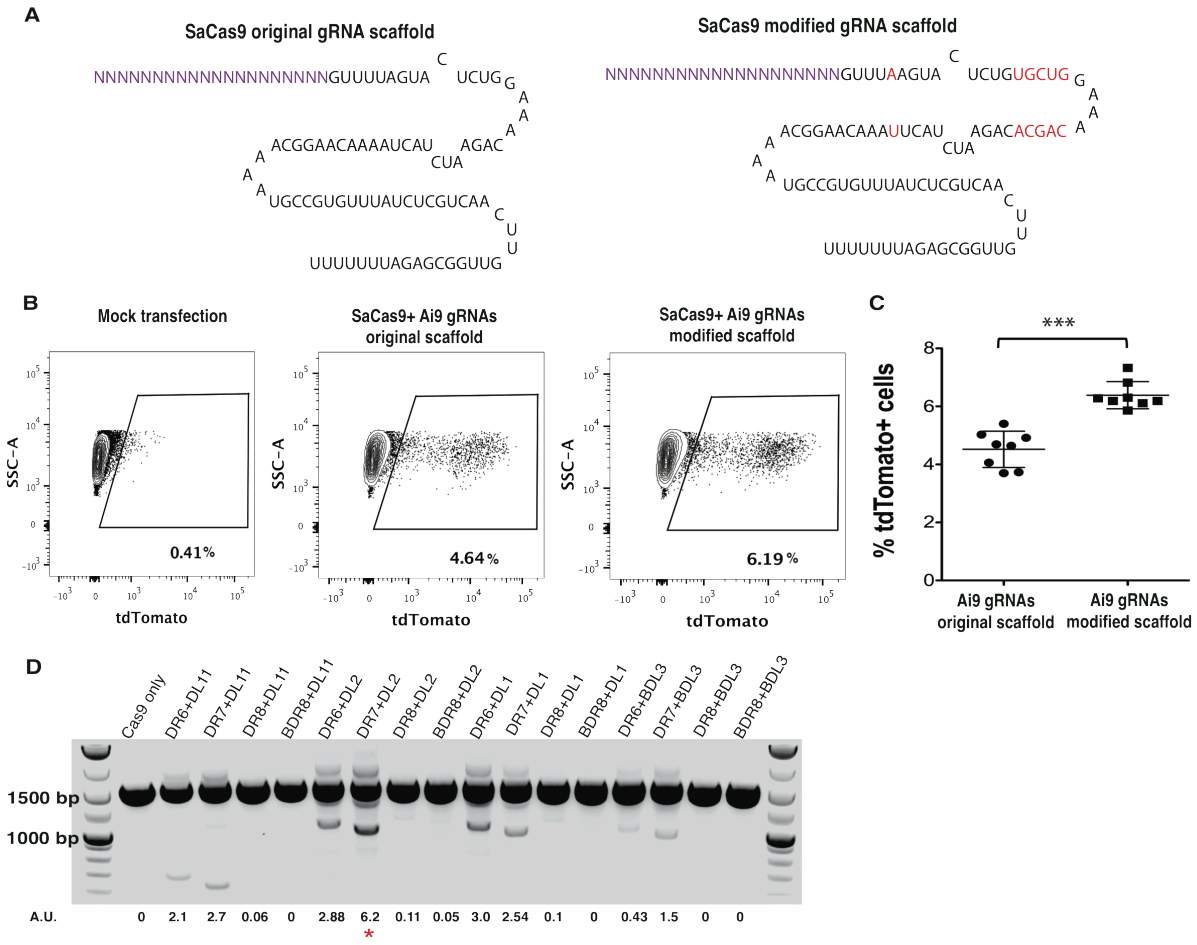
A
SaCas9 original gRNA scaffold
NNNNNNNNNNNNNNNNNNNNGUUUUAGUA UCUG
ACGGAACAAAAUCAU AGAC
CUA
UGCCGUGUUUAUCUCGUCAA
UUUUUUUAGAGCGGUUG
SaCas9 modified gRNA scaffold
NNNNNNNNNNNNNNNNNNNNGUUUAAGUA UCUGUGCUG
ACGGAACAAAUUCAU AGACACGAC
CUA
UGCCGUGUUUAUCUCGUCAA
UUUUUUUAGAGCGGUUG
B
Mock transfection
SaCas9+ Ai9 gRNAs original scaffold
SaCas9+ Ai9 gRNAs modified scaffold
SSC-A
tdTomato
0.41%
4.64%
6.19%
C
***
% tdTomato+ cells
Ai9 gRNAs original scaffold
Ai9 gRNAs modified scaffold
D
Cas9 only
DR6+DL11
DR7+DL11
DR8+DL11
BDR8+DL11
DR6+DL2
DR7+DL2
DR8+DL2
BDR8+DL2
DR6+DL1
DR7+DL1
DR8+DL1
BDR8+DL1
DR6+BDL3
DR7+BDL3
DR8+BDL3
BDR8+BDL3
1500 bp
1000 bp
A.U.
0 2.1 2.7 0.06 0 2.88 6.2 0.11 0.05 3.0 2.54 0.1 0 0.43 1.5 0 0
*

Figure S2. A modified Sa gRNA scaffold results in a higher rate of gene targeting at the Ai9 locus. AAVs are currently in use in human clinical trials (*44, 45*) and provide the opportunity for both local and systemic delivery of virally encoded gene editing complexes *in vivo*; however, the limited packaging capacity of AAVs (4.8 kb) presents an obstacle for their use in delivering large genes such as SpCas9 (4.2kb) (*48, 49*). Use of the orthologous Cas9 protein from *Staphylococcus aureus* (Sa), which is ~1 kb smaller, presents a strategy to overcome this problem (*19*). To further enhance the utility of SaCas9 for *in vivo* gene editing, we modified the SaCas9 gRNA scaffold by incorporating base modifications previously reported to remove a putative RNA polymerase III transcription terminator (*50, 51*) and enhance the assembly of gRNA and catalytically inactive orthologous SpCas9 (*51*). We found that the same base modifications in the gRNA scaffold that increase the efficiency of Sp CRISPR complex formation also enhanced gene targeting by SaCas9 in this system and with this target.

(A) Sequence of the original (left) and modified (right) Sa gRNA scaffold. Base substitutions are noted in red font.

(**B**) Representative FACS plots from Ai9 mouse tail tip fibroblasts transfected with no plasmids (left panel), or with plasmids encoding SaCas9 and Ai9 gRNAs with the original scaffold (middle panel) or the modified scaffold (right panel). Numbers indicate percent TdTomato+ cells.

(**C**) Quantification of percent tdTomato+ targeted cells in transfected Ai9 tail tip fibroblasts transfected with Ai9 gRNAs with the original scaffold or the modified scaffold. Data are plotted as individual data points overlaid with mean ± SD (n=8 per condition). P-value calculated by Mann-Whitney test; ***: $P<0.001$.

(**D**) Result of screening in C2C12 cells of 16 pairs of Sa *Dmd*23 gRNAs, using the modified Sa gRNA scaffold (panel A, right), by genomic PCR using primers spanning exon23. Intensity of the gene-edited band was quantified by densitometry. A.U.: Arbitrary Unit normalized to the unedited band. The combination of DR7+DL2 gRNAs (red asterisk) yielded the highest efficiency of precise DNA excision at exon23, and was therefore chosen for use in further studies.

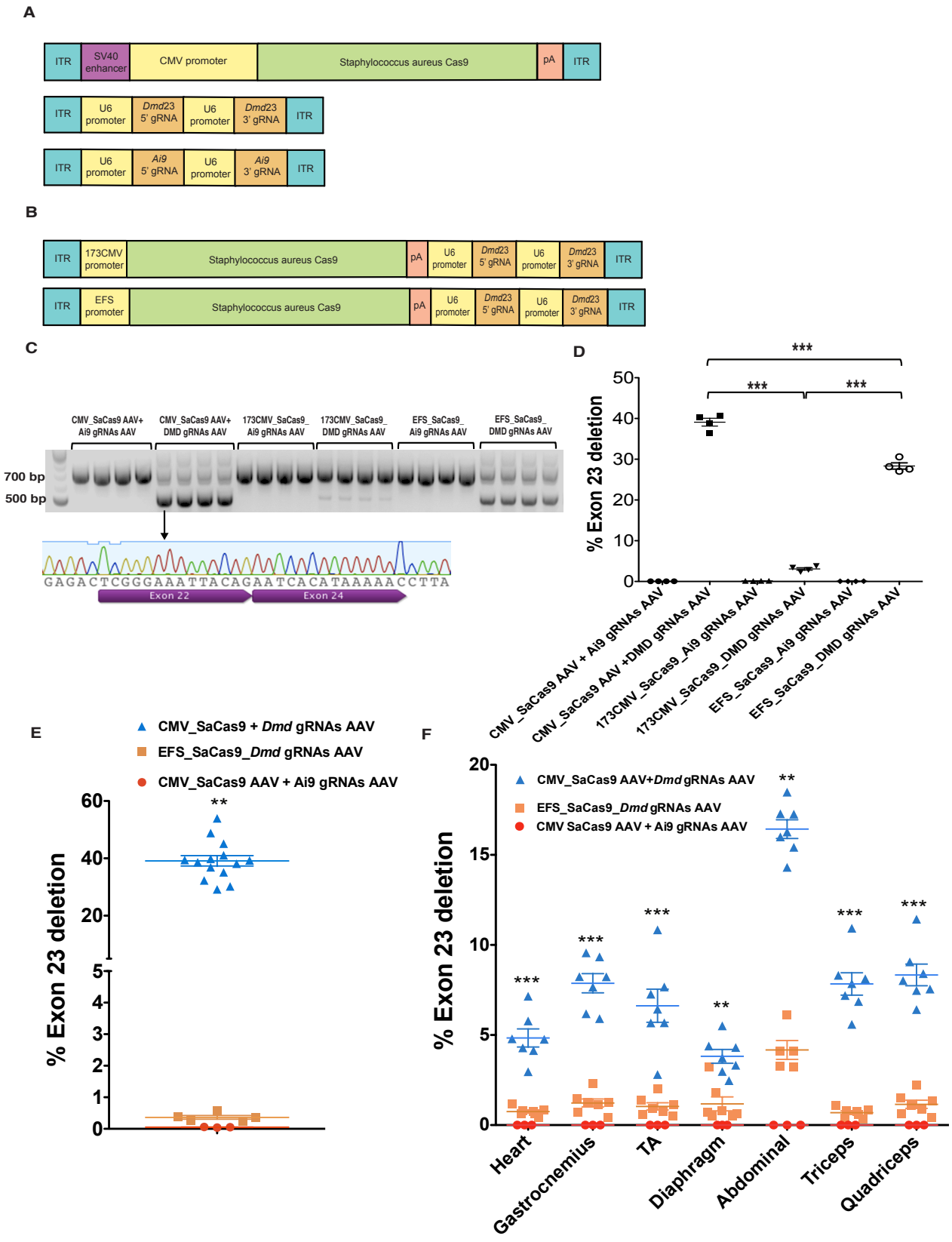
A
ITR
SV40 enhancer
CMV promoter
Staphylococcus aureus Cas9
pA
ITR
ITR
U6 promoter
Dmd23 5' gRNA
U6 promoter
Dmd23 3' gRNA
ITR
ITR
U6 promoter
Ai9 5' gRNA
U6 promoter
Ai9 3' gRNA
ITR
B
ITR
173CMV promoter
Staphylococcus aureus Cas9
pA
U6 promoter
Dmd23 5' gRNA
U6 promoter
Dmd23 3' gRNA
ITR
ITR
EFS promoter
Staphylococcus aureus Cas9
pA
U6 promoter
Dmd23 5' gRNA
U6 promoter
Dmd23 3' gRNA
ITR
C
CMV_SaCas9 AAV+ Ai9 gRNAs AAV
CMV_SaCas9 AAV+ DMD gRNAs AAV
173CMV_SaCas9_ Ai9 gRNAs AAV
173CMV_SaCas9_ DMD gRNAs AAV
EFS_SaCas9_ Ai9 gRNAs AAV
EFS_SaCas9_ DMD gRNAs AAV
700 bp
500 bp
GAGACTCGGGAAATTACAGAATCACATAAAAACCTTA
Exon 22
Exon 24
D
% Exon 23 deletion
50
40
30
20
10
0
***
***
***
CMV_SaCas9 AAV + Ai9 gRNAs AAV
CMV_SaCas9 AAV +DMD gRNAs AAV
173CMV_SaCas9_Ai9 gRNAs AAV
173CMV_SaCas9_DMD gRNAs AAV
EFS_SaCas9_Ai9 gRNAs AAV
EFS_SaCas9_DMD gRNAs AAV
E
CMV_SaCas9 + Dmd gRNAs AAV
EFS_SaCas9_Dmd gRNAs AAV
CMV_SaCas9 AAV + Ai9 gRNAs AAV
% Exon 23 deletion
60
40
20
5
4
3
2
1
0
**
F
CMV_SaCas9 AAV+Dmd gRNAs AAV
EFS_SaCas9_Dmd gRNAs AAV
CMV SaCas9 AAV + Ai9 gRNAs AAV
% Exon 23 deletion
20
15
10
5
0
***
***
***
**
**
***
***
Heart
Gastrocnemius
TA
Diaphragm
Abdominal
Triceps
Quadriceps

Figure S3. Dual AAV-*Dmd* CRISPR constructs target the *Dmd*23 locus more efficiently than single AAV-*Dmd* CRISPR constructs *in vitro* and *in vivo*.

(A) Schematics of AAV-SaCas9 (top) (4728bp including ITRs) AAV-*Dmd23* gRNAs (middle) and AAV-Ai9 gRNAs (bottom) constructs (1393bp including ITRs) used for dual CRISPR AAV experiments. In this system, SaCas9 is expressed from the SV40 enhancer and CMV promoter.

(**B**) Schematics of 173CMV_SaCas9_*Dmd*23 gRNAs (4691bp including ITRs) and EFS_SaCas9_Dmd23 gRNAs (4760bp including ITRs) single AAV constructs. These single vector systems use one of two different small promoters (173CMV (*52*) or elongation factor 1α short (EFS) (*53*)) to drive expression of SaCas9.

(**C**) CRISPR AAV constructs targeting *Dmd*23 (AAV-*Dmd* CRISPR) were used to generate AAV serotype DJ and transduce myotubes differentiated *ex vivo* from *mdx* primary satellite cells in order to compare the efficiency of different constructs for inducing exon23 deletion. RNA was isolated from *mdx;Ai9 in vitro* differentiated myotubes, transduced with AAV DJ encoding the indicated constructs, and exon23 deletion was detected by RT-PCR using primers flanking exon23. Exon23-deleted mRNA was detected only in myotubes receiving AAV-*Dmd* CRISPR. Unedited RT-PCR product: 738bp; exon23-deleted product: 525bp. Sanger sequencing (representative trace shown from the indicated PCR product) confirms the absence of exon23 in the smaller amplicon, in which exon22 is followed in frame by exon24.

(D) Taqman-based quantification of exon23-deleted transcripts in myotubes transduced with AAV DJ encoding dual or single *Dmd*23 CRISPR constructs. Plotted as individual data points overlaid with mean ± SEM, n=4. The EFS-driven SaCas9 was more efficient than the 173CMV-driven SaCas9; however, the dual AAV system induced deletion more efficiently than either of

the single vector constructs. (***: P<0.001, One-way ANOVA followed by the Newman-Keuls multiple comparison test)

(**E**) Taqman-based quantification of exon23-deleted transcripts in TA muscles injected locally (intramuscularly) with dual AAVs encoding SaCas9 + *Dmd*23 gRNAs (7.5E+11 vg each) or single AAV encoding EFS_SaCas9_*Dmd*23 gRNAs (1.5E+12 vg). **: P<0.01 by Mann-Whitney test for comparison of CMV_SaCas9 AAV + *Dmd* gRNAs (blue triangles) to EFS_SaCas9_Dmd gRNAs AAV (orange squares). N=14 for SaCas9 + *Dmd*23 gRNAs injected muscles, n=5 for EFS_SaCas9_*Dmd*23 gRNAs injected muscles and n=3 for SaCas9 + Ai9 gRNAs. Data shown for individual muscles and overlaid with mean ± SEM.

(**F**) Taqman-based quantification of exon23-deleted transcripts in different muscles of mice targeted multisystemically by intraperitoneal injection with dual AAVs encoding SaCas9 + *Dmd*23 gRNAs (1.5E+12 vg each) or single AAV encoding EFS_SaCas9_*Dmd*23 gRNAs (3E+12 vg). Data points for dual AAV injected muscles are reproduced from Fig. 3A for comparison. **: P<0.01 and ***: P<0.001 by Mann-Whitney test for comparison of CMV_SaCas9 AAV + *Dmd* gRNAs (blue triangles) to EFS_SaCas9_Dmd gRNAs AAV (orange squares). N=7 for SaCas9 + *Dmd*23 gRNAs injected muscles, n=5 (abdominal muscle) or 7 (all other muscles) for EFS_SaCas9_*Dmd*23 gRNAs injected muscles and n=3 for SaCas9 + Ai9 gRNAs. Data shown for individual muscles and overlaid with mean ± SEM.

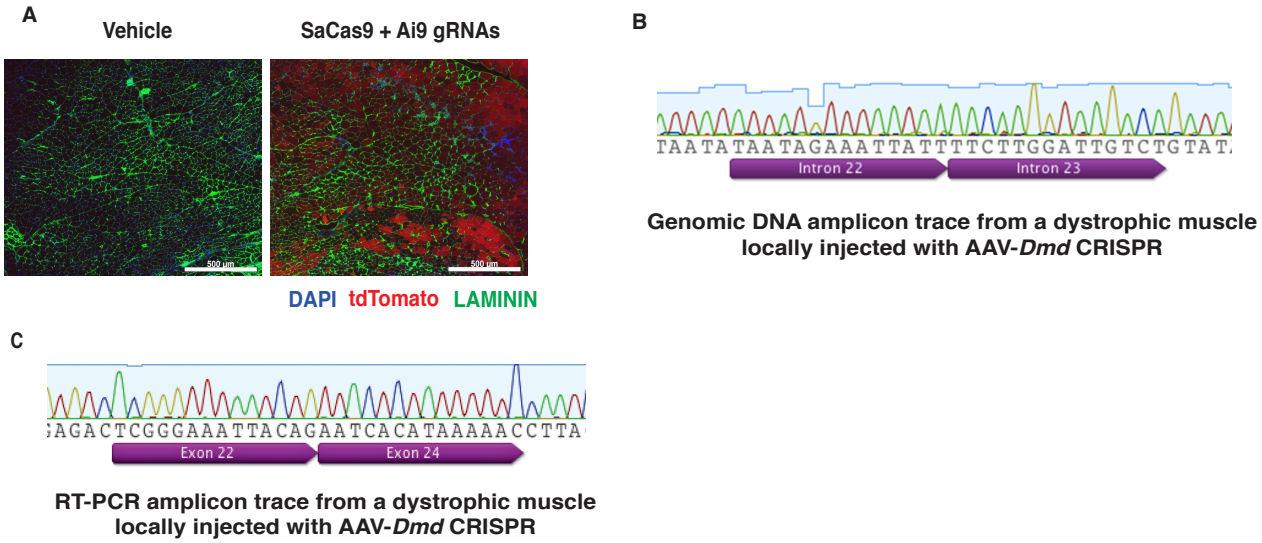

Figure S4. Local, intramuscular delivery of AAV-CRISPR enables *in vivo* genomic modifications in adult dystrophic muscle.

(**A**) Representative immunofluorescence analysis of muscles from adult *mdx;Ai9* mice injected intramuscularly with vehicle (left) or AAV-Ai9 CRISPR (right). TdTomato expression indicates CRISPR activity in muscles receiving AAV-Ai9 CRISPR. Green: LAMININ; Red: tdTomato; Blue: DAPI (nuclei). Scale bar: 500um. We also confirmed that tdTomato was not induced in muscles exposed to AAV-*Dmd* CRISPR, confirming sequence-specific genomic targeting of the CRISPR system (see Fig. S11).

(**B**) Sanger sequencing of amplicons confirms exon23 deletion and generation of a fused intron 22/23 in genomic DNA from TA muscles of *mdx;Ai9* mice injected intramuscularly with AAV-*Dmd* CRISPR. A representative trace is shown from the sample at the far right of the gel in Fig. 2A (red asterisk).

(**C**) Sanger sequencing of RT-PCR amplicons confirms production of an exon23-deleted mRNA transcript, in which exon22 is followed in frame by exon24, in TA muscles of *mdx;Ai9* mice

injected intramuscularly with AAV-*Dmd* CRISPR. A representative trace is shown from the sample at the far right of the gel in Fig. 2B (blue asterisk).

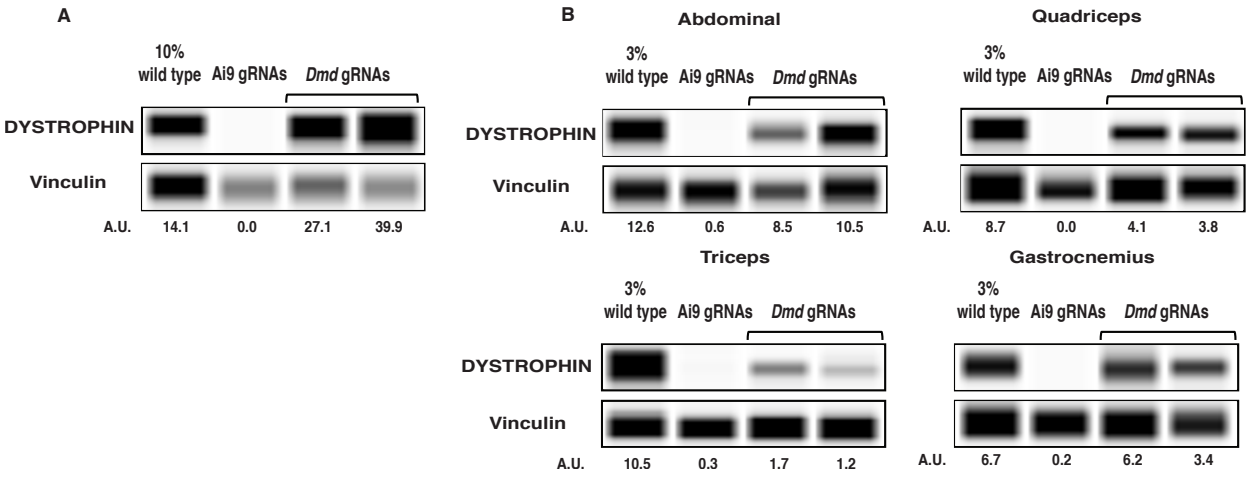

Figure S5. Detection of DYSTROPHIN protein in AAV-*Dmd* CRISPR treated mice using capillary immunoassay from ProteinSimple. To confirm data obtained by classical Western blot analysis (Figs. 2, 3, and S8), a subset of muscle samples was analyzed using ProteinSimple capillary immunoassay technology (ProteinSimple Wes instrument). Data are presented as virtual Western blots for DYSTROPHIN and Vinculin, which serves as a loading control. A.U.: Arbitrary Unit normalized to Vinculin, determined by analysis of chromatograms from each sample.

(**A**) Detection of DYSTROPHIN protein in TA muscles of *mdx;Ai9* mice injected intramuscularly with AAV-CRISPR + *Dmd* gRNA or AAV-CRISPR Ai9 gRNAs as control. Analysis of a sample containing 90% *mdx* + 10% wild-type muscle lysate is provided for comparison. A.U.: Arbitrary Unit normalized to Vinculin.

(**B**) Detection of DYSTROPHIN protein in abdominal, quadriceps, triceps and gastrocnemius muscles of *mdx;Ai9* mice injected intraperitoneally with AAV-CRISPR + *Dmd* gRNA or AAV-CRISPR Ai9 gRNAs as control. Analysis of a sample containing 97% mdx + 3% wild-type muscle lysate is provided for comparison of relative protein levels. A.U.: Arbitrary Unit normalized to Vinculin.

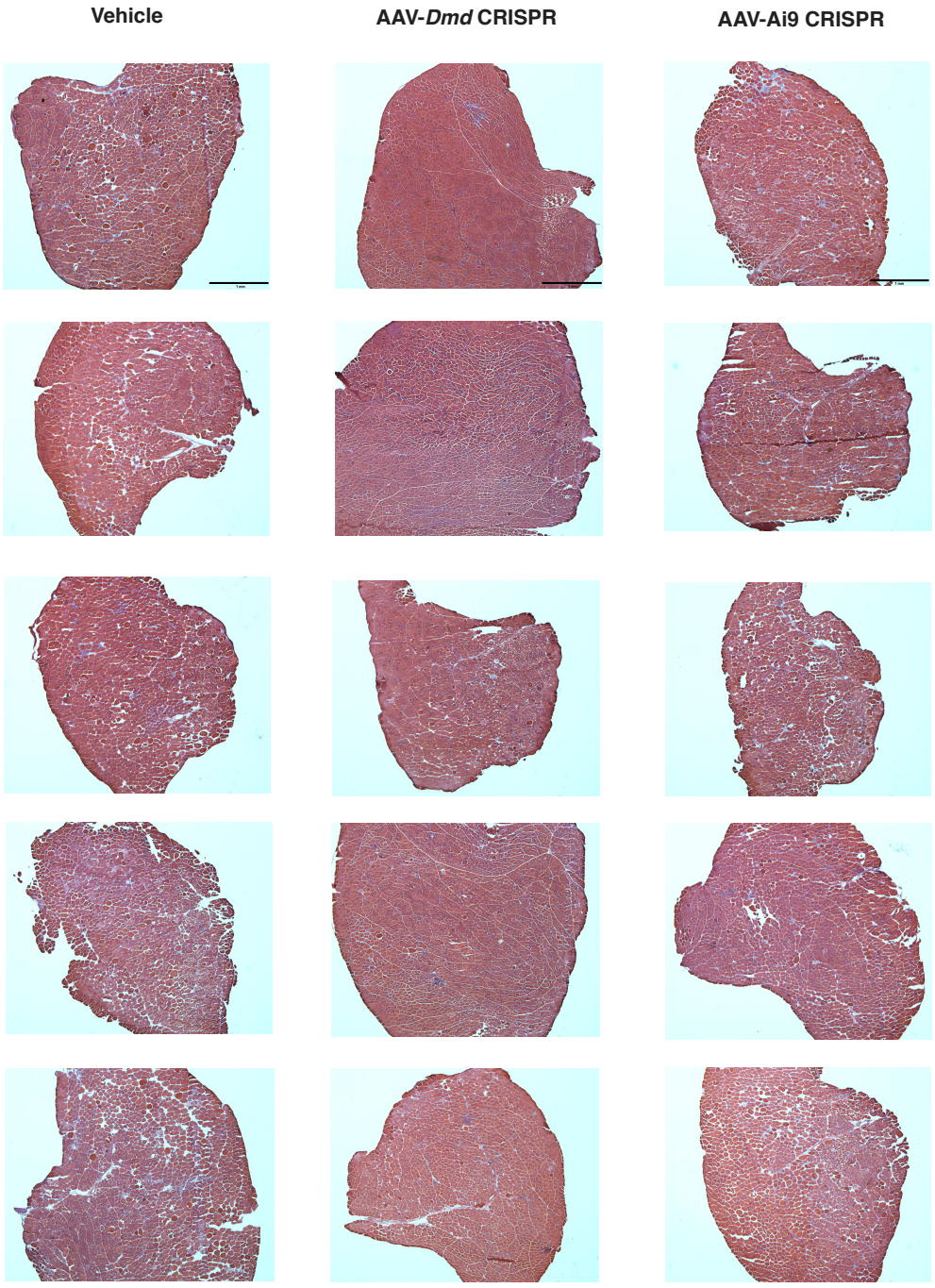

Figure S6. Histological analysis of AAV-CRISPR injected muscles. Representative hematoxylin & eosin (H&E) staining of TA muscle sections from *mdx;Ai9* mice injected intramuscularly with vehicle (left), AAV-*Dmd* CRISPR (middle) or AAV-Ai9 CRISPR (right). Scale bar: 1mm.

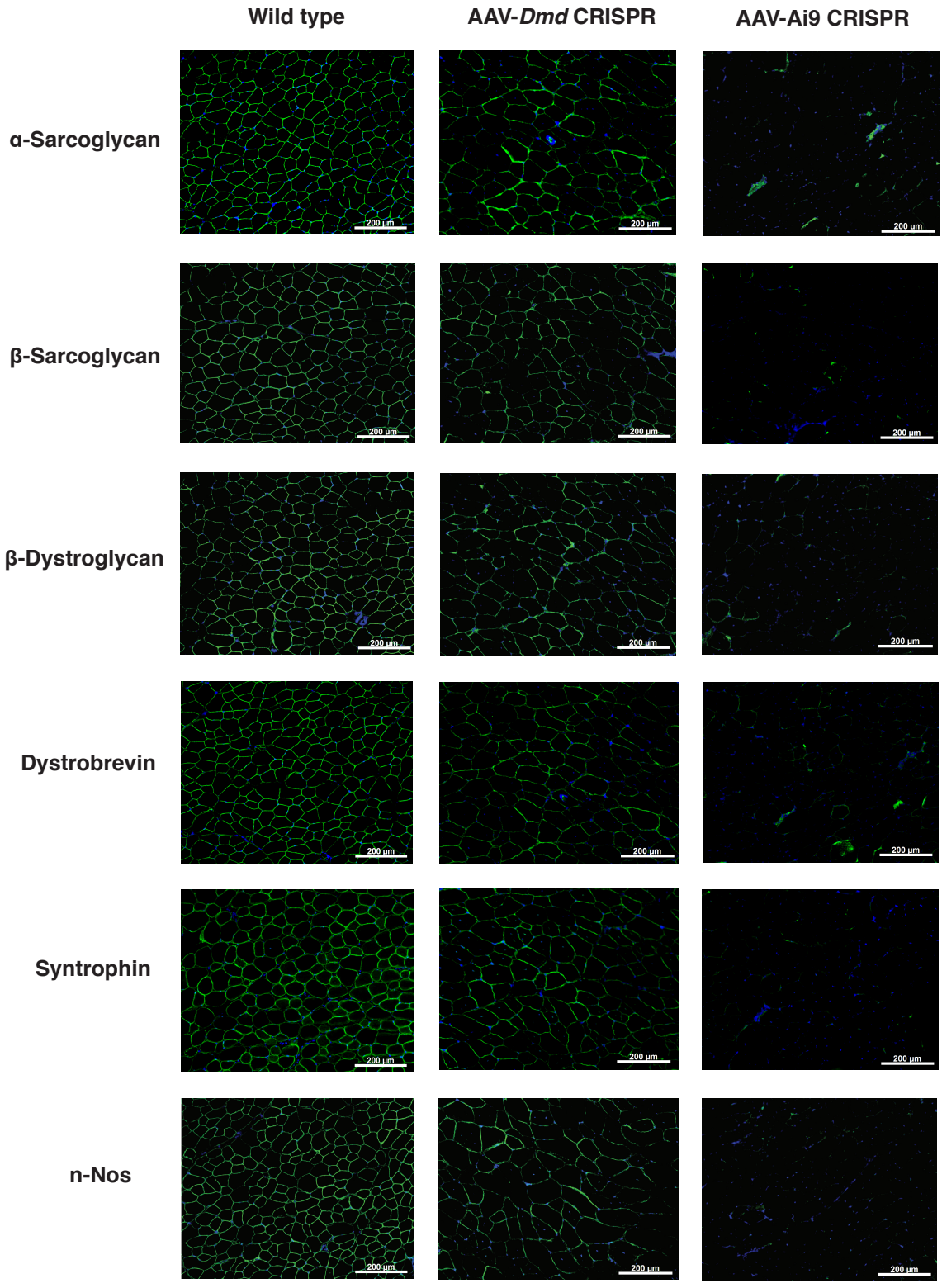
Wild type
AAV-*Dmd* CRISPR
AAV-Ai9 CRISPR
α-Sarcoglycan
β-Sarcoglycan
β-Dystroglycan
Dystrobrevin
Syntrophin
n-Nos
200 µm

Figure S7. Restoration of the dystrophin-glycoprotein (DGC) complex and sarcolemmal nNOS in AAV-*Dmd* CRISPR injected muscles. Immunofluorescence staining for the indicated components of the dystrophin-glycoprotein complex (DGC) or neuronal nitric oxide synthase (nNos) in muscle sections from wild-type mice (left) or *mdx;Ai9* mice injected intramuscularly with AAV-*Dmd* CRISPR (middle) or AAV-Ai9 CRISPR (right). Green: target protein, as indicated at left; Blue: DAPI (nuclei). Scale bar: 200 um.

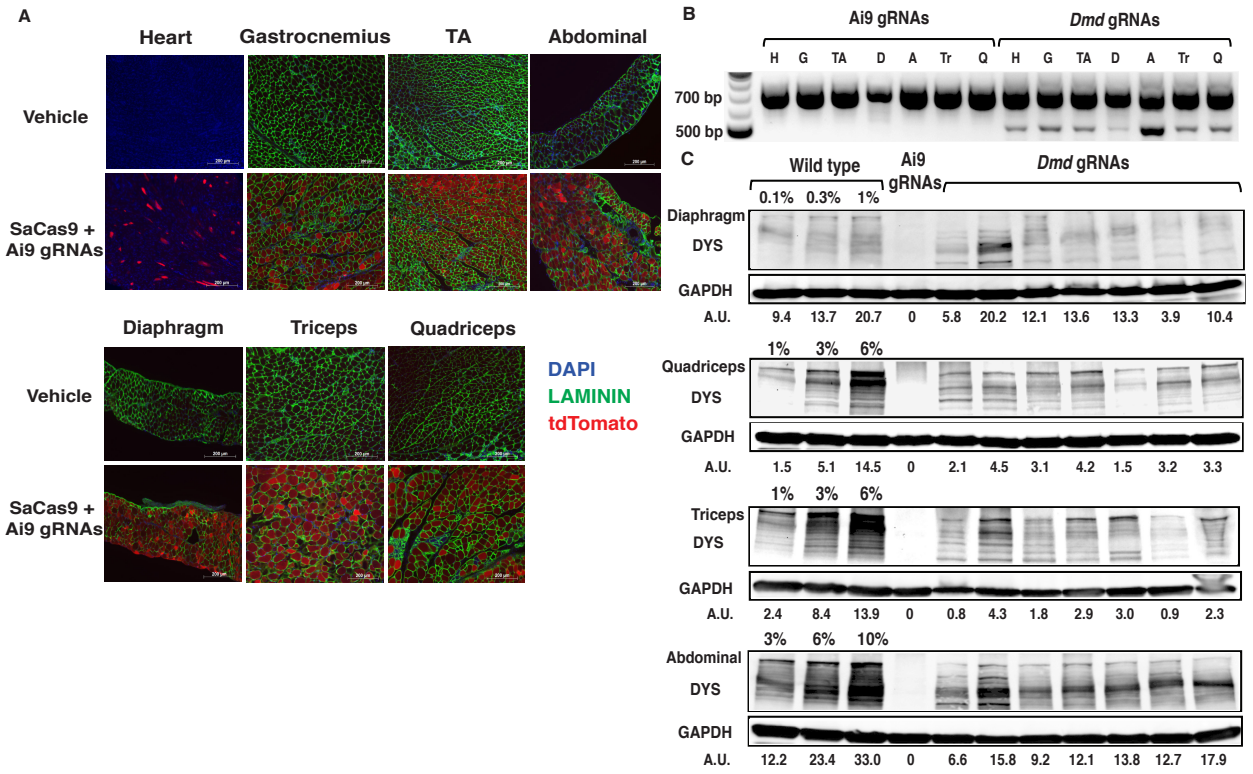

Figure S8. Systemic delivery of AAV-CRISPR in neonatal *mdx* mice targets the Ai9 reporter locus and *Dmd* exon23 and restores DYSTROPHIN expression in cardiac and skeletal muscles.

(**A**) Representative immunofluorescence (Laminin) and epifluorescence (tdTomato) images of muscles from 3 wk. old *mdx;Ai9* mice injected intraperitoneally at postnatal day 3 (P3) with vehicle (top row) or AAV-Ai9 CRISPR (bottom row). TdTomato expression indicates CRISPR activity in muscles receiving SaCas9 + Ai9 gRNAs. Green: LAMININ; Red: tdTomato; Blue: DAPI (nuclei). Scale bar: 200um.

(**B**) Exon23-deleted transcripts are detected in muscles of *mdx;Ai9* mice injected with CRISPR AAVs targeting *Dmd*23 (right), but not Ai9 (left) by RT-PCR.

(**C**) Detection of DYSTROPHIN and GAPDH (loading control) by Western blot in the indicated muscles of 3 week old mice *mdx;Ai9* mice injected intraperitoneally at P3 with AAV-*Dmd* CRISPR. Right lanes correspond to muscles from 7 different mice injected with AAV-*Dmd* CRISPR, as compared to mice injected with AAV-Ai9 CRISPR as control. A titration of muscle cell lysate from wild-type mice (0.1%, 0.3% and 1% wild type protein for diaphragm, 1%, 3% and 6% wild type protein for Quadriceps and Triceps and 3%, 6% and 10% wild type protein for Abdominal) is included for comparison of relative protein levels. Relative signal intensity, determined by densitometry, is given at the bottom. Densitometry for GAPDH in this experiment was performed using a lower exposure blot than that shown here to avoid oversaturation of signal. A.U.: Arbitrary Unit, normalized to GAPDH (loading control). DYS: DYSTROPHIN.

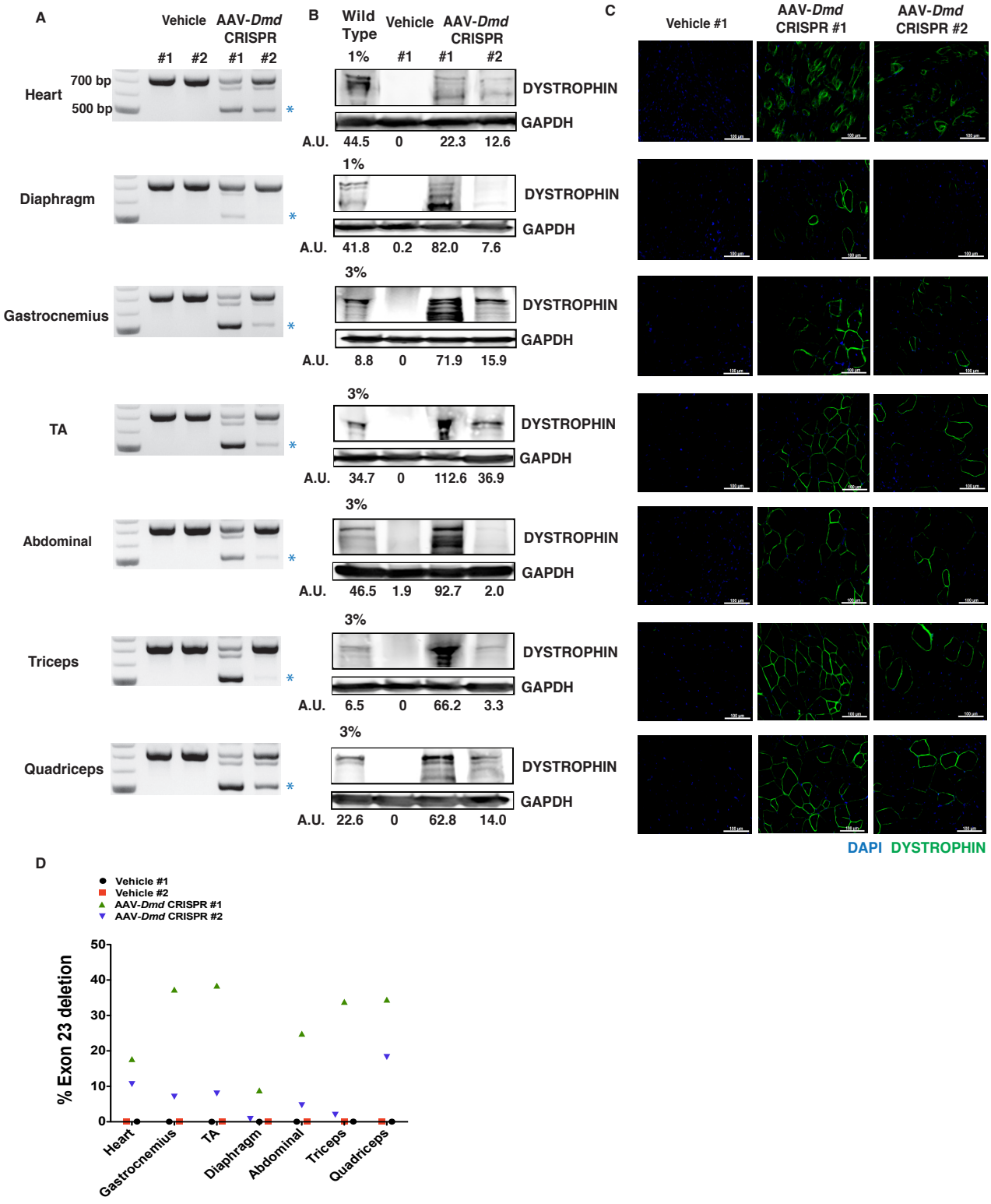
A
Vehicle
AAV-Dmd CRISPR
#1
#2
#1
#2
Heart
700 bp
500 bp
Diaphragm
Gastrocnemius
TA
Abdominal
Triceps
Quadriceps
B
Wild Type
Vehicle
AAV-Dmd CRISPR
1%
3%
DYSTROPHIN
GAPDH
A.U.
44.5 0 22.3 12.6
41.8 0.2 82.0 7.6
8.8 0 71.9 15.9
34.7 0 112.6 36.9
46.5 1.9 92.7 2.0
6.5 0 66.2 3.3
22.6 0 62.8 14.0
C
Vehicle #1
AAV-Dmd CRISPR #1
AAV-Dmd CRISPR #2
DAPI DYSTROPHIN
D
Vehicle #1
Vehicle #2
AAV-Dmd CRISPR #1
AAV-Dmd CRISPR #2
% Exon 23 deletion
50
40
30
20
10
0
Heart
Gastrocnemius
TA
Diaphragm
Abdominal
Triceps
Quadriceps

Figure S9. Systemic delivery of AAV-*Dmd* CRISPR in adult *mdx* mice targets *Dmd* exon23 and restores DYSTROPHIN expression in cardiac and skeletal muscles. Two adult *mdx* mice were injected with 3.6E+13 vg per mouse of AAV-*Dmd* CRISPR at 6 weeks of age. Tissues were harvested for analysis 14 weeks after injection. Similar to results obtained following systemic delivery of AAV-*Dmd* CRISPR in neonatal mice, systemic injection of AAV-*Dmd* CRISPR into adult animals results in multi-organ gene targeting with variable efficiencies in different mice and muscle groups, including cardiac and skeletal muscles.

(A) Exon23-deleted transcripts are detected by RT-PCR in muscles of adult *mdx;Ai9* mice injected with AAV-*Dmd* CRISPR (right lanes), but not with vehicle (left lanes). Unedited RT-PCR product: 738bp; exon23-deleted product (blue asterisk): 525bp.

(B) Detection of DYSTROPHIN and GAPDH (loading control) by Western blot in the indicated muscles of adult *mdx*;Ai9 mice injected intravenously with AAV-*Dmd* CRISPR or vehicle at 6 weeks of age. Third and fourth lanes correspond to muscles from 2 different mice injected with AAV-*Dmd* CRISPR, as compared to a mouse injected with vehicle (second lane). Muscle cell lysate from a wild-type mouse (1% or 3% wild-type proteins) is included for comparison of relative protein levels. Relative signal intensity, determined by densitometry, is given at the bottom. Densitometry for GAPDH in this experiment was performed using a lower exposure blot than that shown here to avoid oversaturation of signal. A.U.: Arbitrary Unit, normalized to GAPDH. Tissue types are indicated at the left side of panel A.

(C) Representative images of immunofluorescence staining for DYSTROPHIN in adult *mdx;Ai9* muscles injected with vehicle or AAV-*Dmd* CRISPR (two different animals shown). Green: DYSTROPHIN; Blue: DAPI (nuclei). Scale bar: 100um. Tissue types are indicated at the left side of panel A.

(D) Quantification of exon23-deleted transcripts in muscles by Taqman-based real time PCR. Data plotted for individual mice (n=2 receiving AAV-*Dmd* CRISPR (blue and green) and n=2 receiving vehicle (black and red).

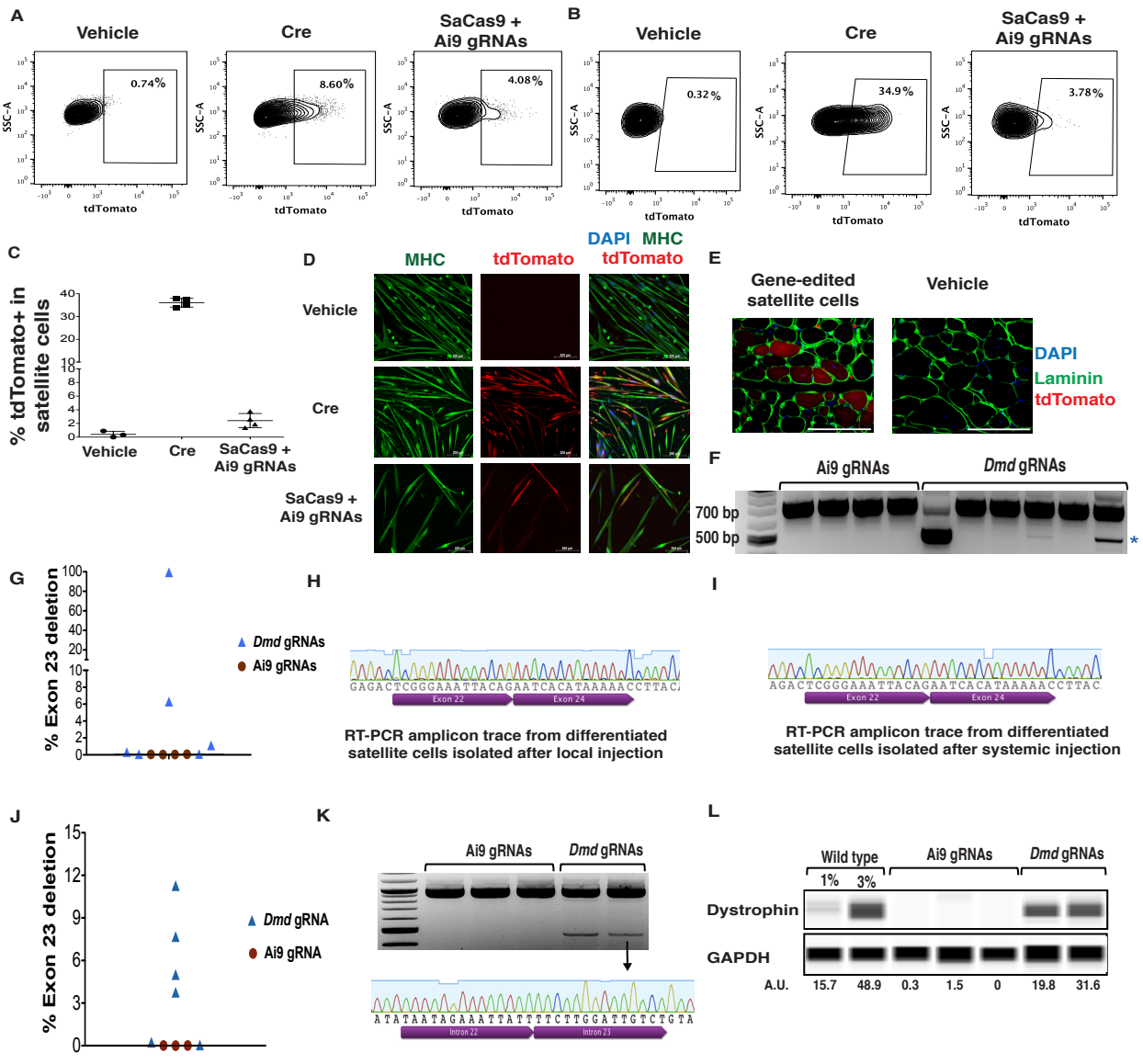

Figure S10. Satellite cells in dystrophic muscles are transduced and targeted with AAV CRISPR injected intramuscularly.

Pax7-ZsGreen$^{+/-}$*;mdx;Ai9* mice were injected intramuscularly or systemically with Cre or CRISPR AAVs targeting Ai9 or *Dmd*23. Two weeks later, Pax7-ZsGreen+ satellite cells were isolated by FACS, expanded in culture, differentiated to myotubes and analyzed for gene editing. (**A**) Representative FACS plots of tdTomato expression among Pax7-ZsGreen+ satellite cells

isolated from *Pax7-ZsGreen*$^{+/-}$*;mdx;Ai9* mice injected intraperitoneally (i.p.) at P3 with vehicle (left), AAV-Cre (middle) or AAV-Ai9 CRISPR (right). Numbers indicate percent tdTomato+ cells for each plot.

(**B**) Representative FACS plots of tdTomato expression among ZsGreen+ satellite cells isolated from mice injected intramuscularly with vehicle (left), AAV-Cre (middle) or AAV-Ai9 CRISPR (right). Numbers indicate percent tdTomato+ cells for each plot.

Excision rates were generally lower for AAV-Ai9 CRISPR than for AAV-Cre, with both systemic (A) and local (B) delivery, possibly reflecting the need for dual AAV transduction in the CRISPR system (see Fig. S3).

(**C**) Quantification of tdTomato+ cells among Pax7-ZsGreen+ satellite cells isolated from mice injected intramuscularly with vehicle, AAV-Cre or AAV-Ai9 CRISPR. Individual data points overlaid with mean ± SD; n=3 mice for vehicle and n=4 mice for Cre and AAV-Ai9 CRISPR. Although a prior study suggested that AAVs do not transduce endogenous satellite cells (*54*), this result likely stems from use of a relatively less sensitive, transient GFP or mCherry expression system for marking transduced cells, in which dilution of the AAV genome during cell division would result in extinction of fluorescence. In contrast, because the AAV-Cre and AAV-CRISPR systems irreversibly mark transduced cells and their progeny, these cells remain distinguishable even after loss of the viral genome, allowing sensitive detection of even very rare *in vivo* gene-modified cells.

(**D**) Representative immunofluorescence images of myotubes differentiated from FACSorted Pax7-ZsGreen+ cells from vehicle (top), AAV-Cre (middle) and AAV-Ai9 CRISPR (bottom) intramuscularly injected muscles. Green: Myosin heavy chain (MHC); Red: tdTomato. Blue: DAPI (nuclei) Scale bar: 200 um.

(**E**) Satellite cells isolated from a dystrophic muscle injected intramuscularly with AAV-Ai9 CRISPR were expanded in culture for two weeks, as described in Materials and Methods and (*18*), and then transplanted into cardiotoxin-preinjured recipient *mdx* mouse muscle (Left). Ten days later, muscles were harvested for immunofluorescence (Laminin, green) and epifluorescence (tdTomato, red) analysis. Detection of tdTomato+ donor-derived myofibers (left image) demonstrates the capacity of gene-edited satellite cells to contribute to muscle regenerative responses *in vivo.* TdTomato+ myofibers were not detected in muscles injected with vehicle only (right image). Scale bar: 100 μm.

(F) RT-PCR with primers flanking exon23 indicates expression of exon23-deleted *Dmd* mRNA in myotubes differentiated *in vitro* from satellite cells isolated from adult TA muscles receiving AAV-*Dmd* CRISPR (right lanes), but not those from muscles injected with AAV-Ai9 CRISPR (left lanes).

(**G**) Taqman quantification of exon23-deleted transcripts in myotubes derived from satellite cells isolated from intramuscularly injected muscles. N=6 mice for AAV-*Dmd* CRISPR and n=4 mice for AAV-Ai9 CRISPR. Variability in % exon23 deletion likely reflects the fact that that only a subset of endogenous satellite cells is transduced by AAV and edited by CRISPR, and as satellite cell recovery from muscle is not absolute, these transduced and targeted cells could be differentially represented in the pool of cells isolated and cultured from each muscle.

(**H**) Sanger sequencing of RT-PCR amplicon confirmed production of an exon23-deleted mRNA transcript, in which exon22 is followed in frame by exon24, in myotubes derived from satellite cells isolated from *Pax7-ZsGreen*$^{+/-}$*;mdx;Ai9* mice injected intramuscularly with AAV-CRISPR targeting *Dmd*23. A representative trace is shown.

(**I**) Sanger sequencing of RT-PCR amplicon confirmed production of an exon23-deleted mRNA transcript, in which exon22 is followed in frame by exon24, in myotubes derived from satellite cells isolated from the TA, gastrocnemius, triceps, quadriceps and abdominal muscles of *Pax7-ZsGreen*$^{+/-}$*;mdx;Ai9* mice injected intraperitoneally with AAV-CRISPR targeting *Dmd*23. A representative trace is shown.

(**J**) Taqman quantification of exon23-deleted transcripts in myotubes derived from satellite cells isolated from the TA, gastrocnemius, triceps, quadriceps and abdominal muscles of *Pax7-ZsGreen*$^{+/-}$*;mdx;Ai9* mice injected intraperitoneally with AAV-CRISPR. N=6 mice for AAV-*Dmd* CRISPR and n=4 mice for AAV-Ai9 CRISPR. Variability in % exon23 deletion likely reflects the fact that that only a subset of endogenous satellite cells is transduced by AAV and edited by CRISPR, and as satellite cell recovery from muscle is not absolute, these transduced and targeted cells could be differentially represented in the pool of cells isolated and cultured from muscles of each mouse.

(**K**) Genomic PCR and sequencing confirming targeted excision of exon23 and generation of a hybrid intron 22/23 in genomic DNA of myotubes derived from satellite cells isolated from *Pax7-ZsGreen*$^{+/-}$*;mdx;Ai9* mice injected intraperitoneally with AAV-CRISPR targeting *Dmd*23. A representative trace is shown from the band indicated by the arrow.

(**L**) Capillary immunoassay analysis (Simple Western, WES instrument, ProteinSimple) indicating restored DYSTROPHIN expression in myotubes derived from satellite cells harvested from mice receiving AAV-*Dmd* CRISPR, but not mice receiving AAV-Ai9 CRISPR. For this experiment, AAV-CRISPR was provided systemically, by intraperitoneal injection into P3 neonatal mice, and satellite cells were isolated from TA, gastrocnemius, triceps, quadriceps and abdominal muscles. Data obtained from ProteinSimple analysis (Wes) are presented as virtual

Western blots for DYSTROPHIN and GAPDH, which serves as a loading control. A.U.: Arbitrary Unit normalized to GAPDH, determined by analysis of chromatograms from each sample.

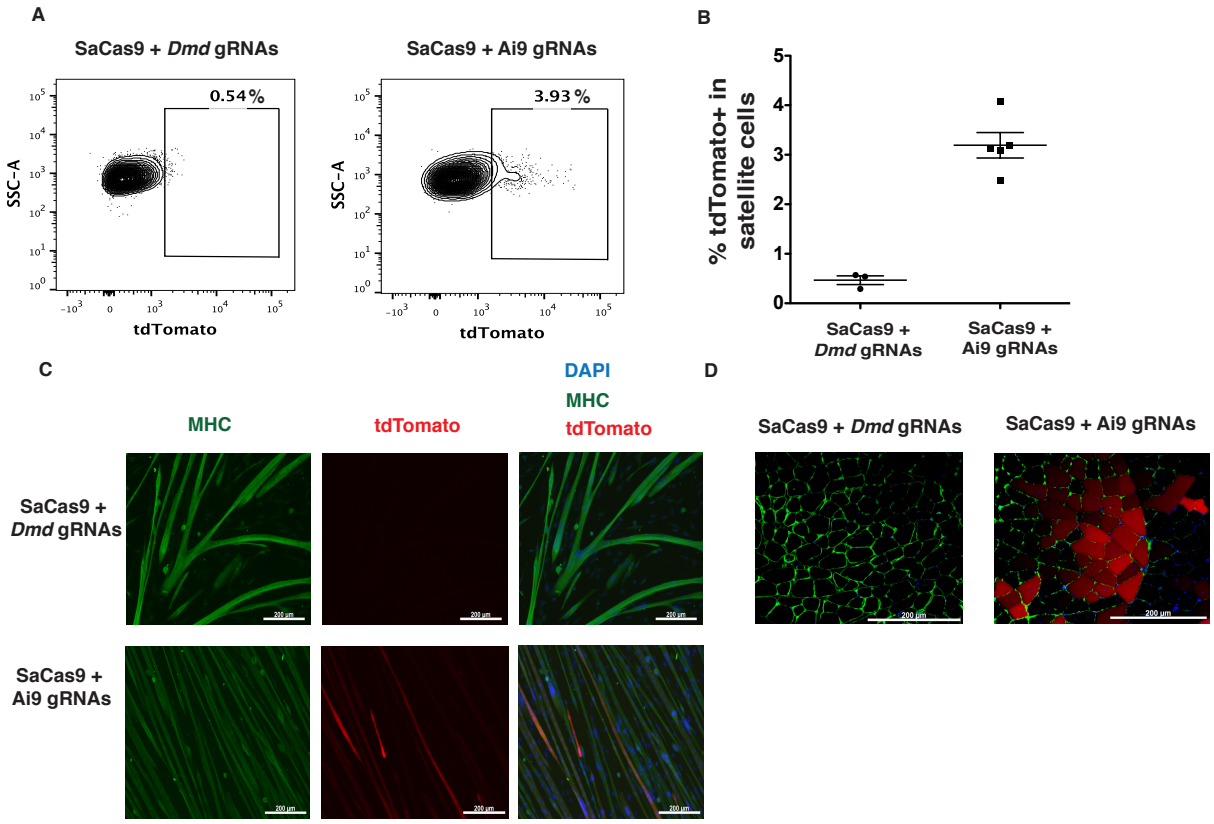

Figure S11. Injection of AAV-*Dmd* CRISPR does not induce tdTomato expression in muscles and satellite cells of *mdx;Ai9* mice.

(A) Representative FACS plots of tdTomato expression among Pax7-ZsGreen+ satellite cells isolated from *Pax7-ZsGreen*$^{+/-}$*;mdx;Ai9* mice injected intraperitoneally at P3 with AAV-*Dmd* CRISPR (left) or AAV-Ai9 CRISPR (right). Numbers indicate percent tdTomato+ cells for each plot.

(B) Quantification of tdTomato+ cells among Pax7-ZsGreen+ satellite cells isolated from mice injected systemically with AAV-*Dmd* CRISPR or AAV-Ai9 CRISPR. Data points for AAV-Ai9 CRISPR injected mice are reproduced from Fig. 4B for comparison. Individual data points

overlaid with mean +/- SD; n=3 mice for AAV-*Dmd* CRISPR and n=5 mice for AAV-Ai9 CRISPR.

(C) Representative immunofluorescence images of myotubes differentiated from FACSorted Pax7-ZsGreen+ cells isolated from AAV-*Dmd* CRISPR (top) and AAV-Ai9 CRISPR (bottom) injected mice. Green: Myosin heavy chain (MHC); Red: tdTomato. Blue: DAPI (nuclei) Scale bar: 200 um.

(D) Representative immunofluorescence analysis of muscles from adult *mdx;Ai9* mice injected intramuscularly with AAV-*Dmd* CRISPR (left) or AAV-Ai9 CRISPR (right). TdTomato expression indicates gene targeting at the Ai9 locus in muscles receiving SaCas9 + Ai9 gRNAs. Editing activity at the Ai9 locus was apparent with AAV-Ai9 CRISPR injection but not with AAV-*Dmd* CRISPR injection. Green: LAMININ; Red: tdTomato; Blue: DAPI (nuclei). Scale bar: 200um.

	#	Sequence	PAM	Chromosome	Position	% Indel (MLE)
Left *Dmd23* gRNA	ON	ATATAATAGAAATTATTCAT	AAGAA	chrX	83803158	2.30782198
	OFF1	ATATAATAAAAATTATTCAT	GGGAG	chr15	29264846	0.00098245
	OFF2	GTTTAATATAAATTATTCAT	TTGAA	chr12	96693430	0.01689232
	OFF3	TTCTATTAGAAATTATTCAT	AGGAA	chr9	39999808	0.00085581
	OFF4	ATAGAATAGTAATTATTCTT	CAGAA	chr2	136343268	0.01360306
	OFF5	GTATACAAGAAATTATTCAT	TTGAA	chr13	114710644	0.02998372
	OFF6	AGATAATAAACATTATTCAT	CAGGG	chr9	65881154	0.01739191
	OFF7	ATATAATTGAAATAATTCAT	CAGAG	chr2	57798779	0.00087477
	OFF8	TTAAAACAGTAATTATTCAT	GTGAA	chrX	121305872	0.00084999
Right *Dmd23* gRNA	ON	CAGTAATGTGTCATACCTTC	TTGGA	chrX	83803700	2.0575122
	OFF1	AGGTAATGTGTCATACTTTC	TGGAG	chrX	165166989	0.00821828
	OFF2	TATTCATATGTCATACCTTC	CAGAA	chr13	112470224	0.01384562
	OFF3	GCTTAATGTATCATACCTTC	CAGGA	chr18	88209239	0.01298753
	OFF4	CACTGATGTGTCATACATTC	TGGAA	chr5	91135977	0.00863797
	OFF5	GTGTCAAGTGTCATACCTTC	ATGAA	chr14	31346645	0.01833734
	OFF6	CATAAAGCTGTCATACCTTC	AGGAA	chr5	90764217	0.00085218
	OFF7	TAGTAATTCTTCATACCTTC	CAGGG	chr13	16839031	0.0042576
	OFF8	CTGTGATATGTCATACCTTT	CAGAA	chr11	10335862	0.01346439

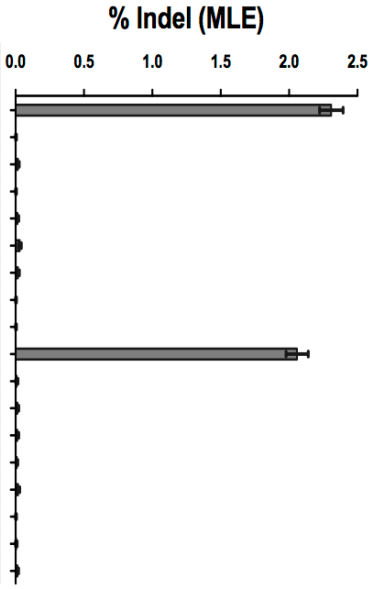

Figure S12. Next generation sequencing analysis of ON- and OFF-target modifications in AAV-CRISPR targeted muscles.

List of predicted off-target sites for the left and right *Dmd*23 gRNAs and the Maximum Likelihood Estimate (MLE) calculated to determine the frequency of on-target and predicted off-target sites with true indels (*28*) in muscles injected with AAV-*Dmd* CRISPR. Targeting efficiency at the on-target sites underestimates CRISPR activity at these sites because deletion of the intervening DNA between the two gRNAs (which leads to recovery of DYSTROPHIN expression) is not detected as an indel by Next generation Sequencing (NGS) due to the large size of the deletion induced. None of the predicted off-target sites are in exonic regions of the genome. n=6 for AAV-*Dmd* CRISPR injected muscles and n=6 for AAV-Ai9 CRISPR injected muscles. AAV-Ai9 CRISPR injected muscles were used as the control for calculating the MLE. Data indicate minimal activity, close to the detection limit of Next Generation Sequencing, at all evaluated off-target sites.

Supplementary Tables (S1-S4)

Table S1- guide RNA target sequences

*Dmd*23 SpCas9 gRNA targets	
Name	Sequence
Sp_Dmd23_L	GAATAATTTCTATTATATTACA
Sp_Dmd23_R	TTCGAAAATTTCAGGTAAGCCG
Ai9 SpCas9 gRNA targets	
Name	Sequence
Sp_Ai9_L	AAAGAATTGATTTGATACCG
Sp_Ai9_R	GTATGCTATACGAAGTTATT
*Dmd*23 SaCas9 gRNA targets	
Name	Sequence
Sa_Dmd23_TL2	ATATAATAGAAATTATTCAT
Sa_Dmd23_TL1	TAATATGCCCTGTAATATAA
Sa_Dmd23_BL3	CAGGGCATATTATATTTAGA
Sa_Dmd23_TR6	CAAAAGCCAAATCTATTTCA
Sa_Dmd23_BR8	TGATATCATCAATATCTTTG
Sa_Dmd23_TR8	GCAATTAATTGGAAAATGTG
Sa_Dmd23_L11	CTTTAAGCTTAGGTAAAATCA
Sa_Dmd23_TR7	CAGTAATGTGTCATACCTTC
Ai9 SaCas9 gRNA targets	
Name	Sequence
Sa_Ai9_L	CTCTAGAGTCGCAGATCCTC
Sa_Ai9_R	ACGAAGTTATATTAAGGGTT

Table S2- Primer and Taqman probe sequences

*Dmd*23 Genomic PCR	
Name	Sequence
Genomic_Dmd23_f	AACAGAACAATTTGACCAAAAACA
Genomic_Dmd23_r	TGGCCAACTATGAGAAACACAAC
Genomic_Dmd23_nested_f	GAGAAACTTCTGTGATGTGAGGAC
Genomic_Dmd23_nested_r	GGTAGTGAAAACATATGTCTGCCA
RT-PCR	
Name	Sequence
RT_Dmd23_f	GACACTTTACCACCAATGCGCTATCAG
RT_Dmd23_r	CTCTAGATATTCTTCTTCAGCTTGTGTCATC
Taqman assay-DMD exon 4-5	
Name	Sequence
E4-5_f	GGCACTGCGGGTCTTACA
E4-5_r	CATCCACTATGTCAGTGCTTCCTAT
E4-5 probe	TTCACTAAATCAACATTATTTTTC
Taqman assay-DMD exon 22-24	
Name	Sequence
E2-24_f	CTGAATATGAAATAATGGAGGAGAGACTCG
E22-24_r	CTTCAGCCATCCATTTCTGTAAGGT
E22-24 probe	ATGTGATTCTGTAATTTCC

Table S3-cloning primers

Name	Sequence
EFS_f	aattcgagctcggtacccGGCTCCGGTGCCCGTCAG
EFS_r	ggcagcgctctagaaccggtCCTGTGTTCTGGCGGCAAAC
saCas9_f	ggttctagagcgctgccaccATGAAAAGGAACTACATTC
saCas9_r	ctgcaataaacaagttGAATTCTTAAGCGTAATCTGGAAC
173cmv_f	aattcgagctcggtacccACTCACGGGGATTTCCAAG
gBlock_f	TGACCCTGAAGTTCATCTGC
gBlock_r	CCTTTCGACCTGCATCCATC
pUC19_f	GGGGATCCTCTAGAGTCGAC
pUC19_r	GGGTACCGAGCTCGAATTCAC

Table S4-gBlock sequences

gBlock1-SV40pA-DmdR7

TGACCCTGAAGTTCATCTGCGAAGACATTTATCGCTTAAGAATTCAACTTGTTTATTGCAGCTT
ATAATGGTTACAAATAAAGCAATAGCATCACAAATTTCACAAATAAAGCATTTTTTTCACTGCATTCTA
GTTGTGGTTTGTCCAAACTCATCAATGTATCTTAGGTACCGAGGGCCTATTTCCCATGATTCCTTCATAT
TTGCATATACGATACAAGGCTGTTAGAGAGATAATTAGAATTAATTTGACTGTAAACACAAAGATATT
AGTACAAAATACGTGACGTAGAAAGTAATAATTTCTTGGGTAGTTTGCAGTTTTAAAATTATGTTTTAA
AATGGACTATCATATGCTTACCGTAACTTGAAAGTATTTCGATTTCTTGGCTTTATATATCTTGTGGAA
AGGACGAAACACCGCAGTAATGTGTCATACCTTCGTTTAAGTACTCTGTGCTGGAAACAGCACAGAAT
CTACTTAAACAAGGCAAAATGCCGTGTTTATCTCGTCAACTTGATAAATGTCTTCGATGGATGCAGGTC
GAAAGG

gBlock2-DmdL2

TGACCCTGAAGTTCATCTGCGAAGACATTTATTGCCGTGTTTATCTCGTCAACTTGTTGGCGAG
ATTTTTTTCCGCGGGAGGGCCTATTTCCCATGATTCCTTCATATTTGCATATACGATACAAGGCTGTTA
GAGAGATAATTAGAATTAATTTGACTGTAAACACAAAGATATTAGTACAAAATACGTGACGTAGAAA
GTAATAATTTCTTGGGTAGTTTGCAGTTTTAAAATTATGTTTTAAAATGGACTATCATATGCTTACCGT
AACTTGAAAGTATTTCGATTTCTTGGCTTTATATATCTTGTGGAAAGGACGAAACACCGACGAAGTTAT
ATTAAGGGTTGTTTAAGTACTCTGTGCTGGAAACAGCACAGAATCTACTTAAACAAGGCAAAATGCCG
TGTTTATCTCGTCAACTTGTTGGCGAGATTTTTTTGGGGATCCTCTAGAGTCGACCTGATAAATGTCTTC
GATGGATGCAGGTCGAAAGG

gBlock3-SV40pA-td_L

TGACCCTGAAGTTCATCTGCGAAGACATTTATCGCTTAAGAATTCAACTTGTTTATTGCAGCTT
ATAATGGTTACAAATAAAGCAATAGCATCACAAATTTCACAAATAAAGCATTTTTTTCACTGCATTCTA
GTTGTGGTTTGTCCAAACTCATCAATGTATCTTAGGTACCGAGGGCCTATTTCCCATGATTCCTTCATAT
TTGCATATACGATACAAGGCTGTTAGAGAGATAATTAGAATTAATTTGACTGTAAACACAAAGATATT
AGTACAAAATACGTGACGTAGAAAGTAATAATTTCTTGGGTAGTTTGCAGTTTTAAAATTATGTTTTAA
AATGGACTATCATATGCTTACCGTAACTTGAAAGTATTTCGATTTCTTGGCTTTATATATCTTGTGGAA
AGGACGAAACACCGCTCTAGAGTCGCAGATCCTCGTTTAAGTACTCTGTGCTGGAAACAGCACAGAAT
CTACTTAAACAAGGCAAAATGCCGTGTTTATCTCGTCAACTTGATAAATGTCTTCGATGGATGCAGGTC
GAAAGG

gBlock4-td_R

TGACCCTGAAGTTCATCTGCGAAGACATTTATTGCCGTGTTTATCTCGTCAACTTGTTGGCGAG
ATTTTTTTCCGCGGGAGGGCCTATTTCCCATGATTCCTTCATATTTGCATATACGATACAAGGCTGTTA
GAGAGATAATTAGAATTAATTTGACTGTAAACACAAAGATATTAGTACAAAATACGTGACGTAGAAA
GTAATAATTTCTTGGGTAGTTTGCAGTTTTAAAATTATGTTTTAAAATGGACTATCATATGCTTACCGT
AACTTGAAAGTATTTCGATTTCTTGGCTTTATATATCTTGTGGAAAGGACGAAACACCGACGAAGTTAT
ATTAAGGGTTGTTTAAGTACTCTGTGCTGGAAACAGCACAGAATCTACTTAAACAAGGCAAAATGCCG
TGTTTATCTCGTCAACTTGTTGGCGAGATTTTTTTGGGGATCCTCTAGAGTCGACCTGATAAATGTCTTC
GATGGATGCAGGTCGAAAGG

Supplementary References and Notes

28. P. D. Hsu, D. A. Scott, J. A. Weinstein, F. A. Ran, S. Konermann, V. Agarwala, Y. Li, E. J. Fine, X. Wu, O. Shalem, T. J. Cradick, L. A. Marraffini, G. Bao, F. Zhang, DNA targeting specificity of RNA-guided Cas9 nucleases. *Nature biotechnology* **31**, 827-832 (2013); published online EpubSep (10.1038/nbt.2647).
29. M. Cerletti, S. Jurga, C. A. Witczak, M. F. Hirshman, J. L. Shadrach, L. J. Goodyear, A. J. Wagers, Highly efficient, functional engraftment of skeletal muscle stem cells in dystrophic muscles. *Cell* **134**, 37-47 (2008); published online EpubJul 11 (
30. R. I. Sherwood, J. L. Christensen, I. M. Conboy, M. J. Conboy, T. A. Rando, I. L. Weissman, A. J. Wagers, Isolation of adult mouse myogenic progenitors: functional heterogeneity of cells within and engrafting skeletal muscle. *Cell* **119**, 543-554 (2004); published online EpubNov 12 (
31. L. V. Anderson, K. Davison, Multiplex Western blotting system for the analysis of muscular dystrophy proteins. *Am J Pathol* **154**, 1017-1022 (1999); published online EpubApr (10.1016/S0002-9440(10)65354-0).
32. L. V. Nicholson, K. Davison, G. Falkous, C. Harwood, E. O'Donnell, C. R. Slater, J. B. Harris, Dystrophin in skeletal muscle. I. Western blot analysis using a monoclonal antibody. *J Neurol Sci* **94**, 125-136 (1989); published online EpubDec (
33. T. J. Burkholder, B. Fingado, S. Baron, R. L. Lieber, Relationship between muscle fiber types and sizes and muscle architectural properties in the mouse hindlimb. *Journal of morphology* **221**, 177-190 (1994); published online EpubAug (10.1002/jmor.1052210207).
34. K. A. Mendez J, Density and composition of mammalian muscle. *Metabolism* **9**, 184-188; published online Epub1960
35. V. Straub, R. E. Bittner, J. J. Leger, T. Voit, Direct visualization of the dystrophin network on skeletal muscle fiber membrane. *J Cell Biol* **119**, 1183-1191 (1992); published online EpubDec
36. K. P. Campbell, S. D. Kahl, Association of dystrophin and an integral membrane glycoprotein. *Nature* **338**, 259-262 (1989); published online EpubMar 16 (10.1038/338259a0).
37. A. Sacco, F. Mourkioti, R. Tran, J. Choi, M. Llewellyn, P. Kraft, M. Shkreli, S. Delp, J. H. Pomerantz, S. E. Artandi, H. M. Blau, Short telomeres and stem cell exhaustion model Duchenne muscular dystrophy in mdx/mTR mice. *Cell* **143**, 1059-1071 (2010); published online EpubDec 23 (
38. N. A. Dumont, Y. X. Wang, J. von Maltzahn, A. Pasut, C. F. Bentzinger, C. E. Brun, M. A. Rudnicki, Dystrophin expression in muscle stem cells regulates their polarity and asymmetric division. *Nat Med*, (2015); published online EpubNov 16 (10.1038/nm.3990).
39. Q. L. Lu, S. Cirak, T. Partridge, What Can We Learn From Clinical Trials of Exon Skipping for DMD? *Molecular therapy. Nucleic acids* **3**, e152 (2014)10.1038/mtna.2014.6).
40. H. Yin, A. F. Saleh, C. Betts, P. Camelliti, Y. Seow, S. Ashraf, A. Arzumanov, S. Hammond, T. Merritt, M. J. Gait, M. J. Wood, Pip5 transduction peptides direct high efficiency oligonucleotide-mediated dystrophin exon skipping in heart and phenotypic correction in mdx mice. *Mol Ther* **19**, 1295-1303 (2011); published online EpubJul (10.1038/mt.2011.79).
41. M. Le Hir, A. Goyenvalle, C. Peccate, G. Precigout, K. E. Davies, T. Voit, L. Garcia, S. Lorain, AAV genome loss from dystrophic mouse muscles during AAV-U7 snRNA-mediated exon-skipping therapy. *Mol Ther* **21**, 1551-1558 (2013); published online EpubAug (10.1038/mt.2013.121).
42. K. M. Flanigan, D. M. Dunn, A. von Niederhausern, P. Soltanzadeh, E. Gappmaier, M. T. Howard, J. B. Sampson, J. R. Mendell, C. Wall, W. M. King, A. Pestronk, J. M. Florence, A. M. Connolly, K. D. Mathews, C. M. Stephan, K. S. Laubenthal, B. L. Wong, P. J. Morehart, A. Meyer, R. S. Finkel, C. G. Bonnemann, L. Medne, J. W. Day, J. C. Dalton, M. K. Margolis, V. J. Hinton, R. B. Weiss, Mutational spectrum of DMD mutations in dystrophinopathy patients: application of modern diagnostic techniques to a large cohort. *Human mutation* **30**, 1657-1666 (2009); published online EpubDec (10.1002/humu.21114).
43. C. Beroud, S. Tuffery-Giraud, M. Matsuo, D. Hamroun, V. Humbertclaude, N. Monnier, M. P. Moizard, M. A. Voelckel, L. M. Calemard, P. Boisseau, M. Blayau, C. Philippe, M. Cossee, M. Pages, F. Rivier, O. Danos, L. Garcia, M. Claustres, Multiexon skipping leading to an artificial DMD protein lacking amino acids from exons 45 through 55 could rescue up to 63% of patients with Duchenne muscular dystrophy. *Hum Mutat* **28**, 196-202 (2007); published online EpubFeb (10.1002/humu.20428).
44. M. A. Kotterman, D. V. Schaffer, Engineering adeno-associated viruses for clinical gene therapy. *Nat Rev Genet* **15**, 445-451 (2014); published online EpubJul (10.1038/nrg3742).

45. F. Mingozzi, K. A. High, Therapeutic in vivo gene transfer for genetic disease using AAV: progress and challenges. *Nat Rev Genet* **12**, 341-355 (2011); published online EpubMay (10.1038/nrg2988).
46. C. E. Nelson, C. H. Hakim, D. G. Ousterout, P. I. Thakore, E. A. Moreb, R. Castellanos, S. Madhavan, X. Pan, F. A. Ran, W. X. Yan, A. Asokan, F. Zhang, D. Duan, C. A. Gersbach, In vivo genome editing imporves muscle function in a model of Duchenne muscular dystrophy. (submitted).
47. E. Zinn, S. Pacouret, V. Khaychuk, H. T. Turunen, L. S. Carvalho, E. Andres-Mateos, S. Shah, R. Shelke, A. C. Maurer, E. Plovie, R. Xiao, L. H. Vandenberghe, In Silico Reconstruction of the Viral Evolutionary Lineage Yields a Potent Gene Therapy Vector. *Cell reports* **12**, 1056-1068 (2015); published online EpubAug 11 (10.1016/j.celrep.2015.07.019).
48. Z. Wu, H. Yang, P. Colosi, Effect of genome size on AAV vector packaging. *Mol Ther* **18**, 80-86 (2010); published online EpubJan (10.1038/mt.2009.255).
49. J. Y. Dong, P. D. Fan, R. A. Frizzell, Quantitative analysis of the packaging capacity of recombinant adeno-associated virus. *Hum Gene Ther* **7**, 2101-2112 (1996); published online EpubNov 10 (10.1089/hum.1996.7.17-2101).
50. S. Nielsen, Y. Yuzenkova, N. Zenkin, Mechanism of eukaryotic RNA polymerase III transcription termination. *Science* **340**, 1577-1580 (2013); published online EpubJun 28 (10.1126/science.1237934).
51. B. Chen, L. A. Gilbert, B. A. Cimini, J. Schnitzbauer, W. Zhang, G. W. Li, J. Park, E. H. Blackburn, J. S. Weissman, L. S. Qi, B. Huang, Dynamic imaging of genomic loci in living human cells by an optimized CRISPR/Cas system. *Cell* **155**, 1479-1491 (2013); published online EpubDec 19 (10.1016/j.cell.2013.12.001).
52. L. S. Ostedgaard, T. Rokhlina, P. H. Karp, P. Lashmit, S. Afione, M. Schmidt, J. Zabner, M. F. Stinski, J. A. Chiorini, M. J. Welsh, A shortened adeno-associated virus expression cassette for CFTR gene transfer to cystic fibrosis airway epithelia. *Proc Natl Acad Sci U S A* **102**, 2952-2957 (2005); published online EpubFeb 22 (10.1073/pnas.0409845102).
53. O. Shalem, N. E. Sanjana, E. Hartenian, X. Shi, D. A. Scott, T. S. Mikkelsen, D. Heckl, B. L. Ebert, D. E. Root, J. G. Doench, F. Zhang, Genome-scale CRISPR-Cas9 knockout screening in human cells. *Science* **343**, 84-87 (2014); published online EpubJan 3 (10.1126/science.1247005).
54. A. L. Arnett, P. Konieczny, J. N. Ramos, J. Hall, G. Odom, Z. Yablonka-Reuveni, J. R. Chamberlain, J. S. Chamberlain, Adeno-associated viral (AAV) vectors do not efficiently target muscle satellite cells. *Mol Ther Methods Clin Dev* **1**, (2014)10.1038/mtm.2014.38).